
Decoupled Self-supervised Learning for Non-Homophilous Graphs

Teng Xiao¹, Zhengyu Chen², Zhimeng Guo¹, Zeyang Zhuang³, Suhang Wang¹

¹The Pennsylvania State University, ²Zhejiang University, ³Tongji University
{tengxiao, zhimeng, szw494}@psu.edu, chenzhengyu@zju.edu.cn
zeyangzhuang0315@gmail.com

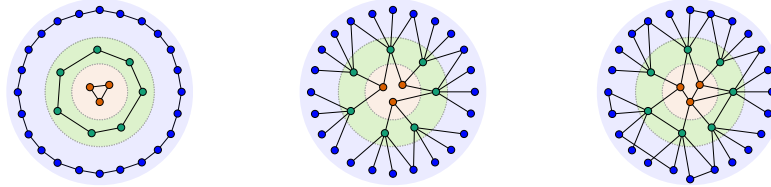
Abstract

In this paper, we study the problem of conducting self-supervised learning for node representation learning on non-homophilous graphs. Existing self-supervised learning methods typically assume the graph is homophilous where linked nodes often belong to the same class or have similar features. However, such assumptions of homophily do not always hold true in real-world graphs. We address this problem by developing a decoupled self-supervised learning (DSSL) framework for graph neural networks. DSSL imitates a generative process of nodes and links from latent variable modeling of the semantic structure, which decouples different underlying semantics between different neighborhoods into the self-supervised node learning process. Our DSSL framework is agnostic to the encoders and does not need prefabricated augmentations, thus is flexible to different graphs. To effectively optimize the framework with latent variables, we derive the evidence lower-bound of the self-supervised objective and develop a scalable training algorithm with variational inference. We provide a theoretical analysis to justify that DSSL enjoys better downstream performance. Extensive experiments on various types of graph benchmarks demonstrate that our proposed framework can significantly achieve better performance compared with competitive self-supervised learning baselines.

1 Introduction

Graph-structured data is ubiquitous in real world such as social networks, knowledge graphs, and molecular structures. In recent years, graph neural networks (GNNs) [13, 25, 45, 50] have been proven to be powerful in node representation learning over graph-structured data and have achieved state-of-the-art performance across various tasks such as node classification. Typically, GNNs are trained with annotated labeled data in a supervised manner. However, collecting labeled data is expensive and impractical in many applications, especially for those requiring domain knowledge for annotation, such as medicine and chemistry [60, 17]. Moreover, supervised learning with labeled data may suffer from problems of less-transferrable, over-fitting and poor generalization particularly when the task-specific labels are scarce [7, 53].

Recently, self-supervised learning (SSL) provides a promising learning paradigm that reduces the dependence on manual labels in the image domain [5, 9, 10, 16]. Compared to image data, there are unique challenges of designing self-supervised learning schemes for graph-structured data since nodes in the graph are correlated with each other rather than completely independent, and geometric structures are essential and heavily impact the performance in downstream tasks [25]. A number of recent works [46, 15, 53, 59, 41, 55] have studied graph self-supervised learning and confirm that it can learn transferrable and generalizable node representations without any labels. Typically, there are two main self-supervised schemes to capture structure information in graphs [46, 53, 39]. The first scheme is reconstructing the vertex adjacency following traditional network-embedding methods [24, 11, 14, 13, 40], which learns an encoder that imposes the topological closeness of nodes in the graph structure on latent representations. The key assumption behind this scheme is that neighboring nodes have similar representations [46, 40]. However, this assumption over-emphasizes proximity [46, 53] and does not hold true for heterophilic and non-homophilous (mixing) graphs where linked nodes may have dissimilar features and different class labels. In comparison, contrastive



(a) Graph with homophilous pattern. (b) Graph with heterophilic pattern. (c) Graph with mixing pattern.

Figure 1: An illustration examples of different types of graphs. We can find nodes with similar labels typically have similar neighborhood patterns in all types of graph. This assumption is more general than the standard homophily assumption where nodes with similar semantic label typically be linked with each other.

learning methods [46, 15, 53, 59, 41] constructs two graph views via the stochastic augmentation and then learns representations by contrasting views with information maximization principle. While these contrastive methods can capture structure information without directly emphasizing proximity, their performance heavily relies on the topology augmentation and negative sample mining [58, 43]. Importantly, conducting augmentation and negative sample mining for non-homophilous or even extreme heterophilic graphs is difficult since linked nodes may be dissimilar and nodes with high similarities might be farther away from each other. As shown in our experiments in Table 1, most of contrastive learning methods fail to generalize to non-homophilous graphs. Although there are many efforts [32, 57, 27, 59, 6, 51] trying to deal with the non-homophilous graph by designing new GNN models, they are still supervised learning approaches and heavily rely on the annotated labels, which limits their applications where labeled data is expensive and unavailable. Hence, the above problems pose an important and challenging research question: *How to design an effective self-supervised scheme for node representation learning in non-homophilous graphs?*

We approach this question by investigating whether one can take advantage of neighborhood strategies of nodes to help the self-supervised learning for non-homophilous graphs. Our key motivation is that nodes with similar neighborhood patterns should have similar representations. In other words, we expect that the neighborhood distributions can be exploited to distinguish node representations. Our assumption is more general than the standard homophily assumption. For instance, while the gender prediction in common dating networks lacks homophily (individual with gender male has a preference of making friends with people whose identities are female) [1], neighborhood distribution are very informative to the node gender labels, i.e., nodes with similar neighborhoods are likely to be similar. Figure 1 illustrates this motivation.

While the motivation is straightforward, there are two challenges to achieve it. The first challenge is how to capture the local neighborhood distribution in a self-supervised learning manner. The neighborhood distributions typically follow heterogeneous and diverse patterns. For instance, as shown in Figure 2 (c), a node usually connects with others due to the complex interaction of many latent factors, and therefore possesses distribution consisting of local mixing patterns wherein certain parts of the neighborhood are homophilous while others non-homophilous. Since there is no way to directly access the latent strategies of neighborhoods, the lack of supervision obstructs us from modeling the distribution of neighborhood. The second challenge is capturing the long-range semantic dependencies in self-supervised learning objectives. As shown in Figure 2, in non-homophilous graphs, nodes with high semantic and local structural similarities might be farther away from each other. For this reason, global semantic information is the objective that we would incorporate for self-supervised learning, due to its favorable performance in downstream task.

This paper presents a new self-supervised framework: the decoupled self-supervised learning (DSSL), which attempts to achieve a good balance among these two challenges. At the core of DSSL is the latent variables, which empower model the flexibility to decouple the heterogeneous and diverse patterns in local neighborhood distributions and capture the global semantic dependencies in a coherent and synergistic framework. Our contributions can be summarized as follows: (1) We propose a unified DSSL framework for performing self-supervised learning on non-homophilous graphs, which can leverage both useful local structure and global semantic information. (2) We develop an efficient training algorithm based on variational inference to simultaneously infer the latent variables and learn encoder parameters. (3) We analyze the properties of DSSL and theoretically show that the learned representations can achieve better downstream performance. (4) We conduct experiments on real-world non-homophilous graphs including large-scale ones and the results demonstrate the effectiveness of our self-supervised learning framework.

2 Related Work

Non-homophilous Graphs. Non-homophilous is known in many settings such as online transaction networks [31], dating networks [1] and molecular networks [57]. Recently, various GNNs have been proposed to

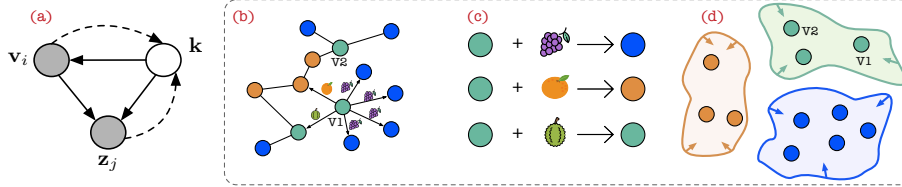


Figure 2: An illustration of (a) graphical model for DSSL. The latent variable k is used to instantiate a latent mixture-of-Gaussians v_i , which is then decoded to z_j and (b) a toy subgraph example of non-homophilous graphs. The motivation behind this work. (c) Our model encodes the semantic shift by decoupling local structure and (d) captures global semantic structure by semantic clusters.

deal with non-homophilous graphs with different methods such as potential neighbor discovery [32, 21, 19], adaptive message propagation [6, 49], exploring high-frequency signals [2] and higher-order message passing [57, 5]. Despite their success, they typically consider the semi-supervised setting and are trained with task-specific labeled data; while in practice, labels are often limited, expensive, and even inaccessible. In contrast, in this paper, we study the problem of self-supervised learning: learning generalizable and transferable node representations without relying on labels for non-homophilous graphs.

Self-supervised Learning on Graphs. Self-supervised learning holds great promise for improving representations when labeled data are scarce [5, 9, 10, 16]. In graph domain, earlier combinations of GNNs and self-supervised learning involve GraphSAGE [13], VGAE [24] and Graphite [12], which typically follow the traditional network-embedding methods [34, 40, 11] and adopt the link reconstruction or random walk principle. Since these methods over-emphasize node proximity at the cost of structural information [46, 39, 53], various graph contrastive learning methods have been proposed [46, 15, 53, 59, 41], which aim to learn representations by contrasting representation under differently augmented views and have achieved promising performance. However, they heavily rely on complex data- or task-specific augmentations, which are prohibitively difficult for non-homophilous graphs. The standard augmentation scheme usually has limited performance for non-homophilous graphs as shown in our experiments. There are also some recent works trying to design heuristic pretext tasks [54, 20, 17] on graphs, however, for non-homophilous graphs, building hand-crafted pretext tasks for each node tends to be infeasible when we know little knowledge underlying graph or the node has diverse context. Our work differs from the above methods and aims to answer the question of how to design effective self-supervised learning scheme for non-homophilous graphs.

Disentangled graph learning. Our work is also related but different from existing disentangled graph learning that aims to disentangle latent factors in the graph. There are a couple of works that explore the disentangled factors in the node-level [30, 29], edge-level [56] and graph-level [52]. Whereas, these methods require task-specific labels that can be extremely scarce for graph datasets. By contrast, we address the problem of learning generalizable and transferrable node representations on non-homophilous graphs without labels. A recent work called disentangled contrastive learning [26] learns disentangled graph representations without labeled graph. Nevertheless, they are still based on contrastive learning which requires prefabricated augmentations. By contrast, our framework is a generative model and does not rely on graph augmentations. Moreover, their goal is to conduct graph-level classification tasks which are different from ours. We instead tackle a node-level representation problem on non-homophilous graphs where connected nodes may not be similar to each other and we decouple the diverse neighborhood context of a node with a generative process.

3 Decoupled Self-supervised Learning

In this section, we describe our problem setting, and demonstrate our approach. An illustration of and inference processes is depicted in Figure 2 (a).

3.1 Problem Formulation

We consider a graph $G = (\mathcal{V}, \mathcal{E})$, where \mathcal{V} is a set of $|\mathcal{V}| = N$ nodes and $\mathcal{E} \subseteq \mathcal{V} \times \mathcal{V}$ is a set of $|\mathcal{E}|$ edges between nodes. $\mathbf{A} \in \{0, 1\}^{N \times N}$ is the adjacency matrix of G . The (i, j) -th element $\mathbf{A}_{ij} = 1$ if there exists an edge (v_i, v_j) between node v_i and v_j , otherwise $\mathbf{A}_{ij} = 0$. The matrix $\mathbf{X} \in \mathbb{R}^{N \times D}$ is used to describe node features. The i -th row of \mathbf{X} , i.e., \mathbf{x}_i , is the feature vector of node v_i . Given the graph $\mathcal{G} = (\mathbf{X}, \mathbf{A})$, the objective of self-supervised node representation learning is to learn an encoder function $f_\theta(\mathbf{X}, \mathbf{A}) : \mathbb{R}^{N \times N} \times \mathbb{R}^{N \times D} \rightarrow \mathbb{R}^{N \times D'}$ where θ denotes the set of its parameters, such that the representation of node v_i , i.e., $f_\theta(\mathbf{X}, \mathbf{A})[i]$, can be used for downstream tasks.

3.2 The Probabilistic Framework

In this section, we introduce our framework, decoupled self-supervised learning (DSSL), which can learn meaningful node representations for non-homophilous graphs by capturing its intrinsic graph structure. The core idea of DSSL is to model the distributions of node neighbors via a mixture generative process in the representation learning scenario. Specifically, we model the generation of neighbors by assuming each node has latent heterogeneous factors which are utilized to make connections to its different neighbors. Intuitively, the factor denotes various reasons behind why two nodes are connected. For instance, two nodes in a school network will be connected depending on some factors such as colleagues, friends or classmates; in protein networks, even if they do not have similar features, different amino acid types are likely to be connected due to various interactions.

Formally, let $f_\theta(\mathbf{X}, \mathbf{A})[i] = \mathbf{v}_i$ and $f_\theta(\mathbf{X}, \mathbf{A})[j] = \mathbf{z}_j$ be the representations of nodes v_i and v_j , respectively. Here we utilize different notations, i.e., \mathbf{v} and \mathbf{z} to distinguish between central and neighbor nodes since each node plays two roles: the node itself and a specific neighbor of other nodes. Our goal is to find the encoder parameter θ which maximizes the likelihood of distribution $p(\mathbf{z}_j|\mathbf{v}_i; \theta)$ on central node and its neighbor. To model the unobserved factors, we associate every node \mathbf{v}_i with a discrete latent variable k to indicate to which factor \mathbf{v}_i has. Assume that there are K factors in total, the log-likelihood of node neighbors \mathbf{v}_i can be written by marginalizing out the latent variables:

$$\mathcal{L}_{DSSL}(\theta) = \frac{1}{|N(i)|} \sum_{j \in N(i)} \log[p_\theta(\mathbf{z}_j|\mathbf{v}_i)] = \frac{1}{|N(i)|} \sum_{j \in N(i)} \log \left[\sum_{k=1}^K p_\theta(\mathbf{z}_j|\mathbf{v}_i, k) p_\theta(k|\mathbf{v}_i) \right], \quad (1)$$

where $N(i)$ is the set of out-neighbors of v_i , the distribution $p_\theta(k|\mathbf{v}_i)$ indicates the assignment of latent semantics over central node representation \mathbf{v}_i , and $p_\theta(\mathbf{z}_j|\mathbf{v}_i, k)$ is the probability that node v_i and its neighbor v_j are connected under factor k . Unlike previous works [34, 40, 11, 24], which directly encourages nearby nodes to have similar representations, we provide an alternative way to model node neighbors, and seek to decouple their latent relationship without any prior on neighbor partitions, so that the model is more generalizable for non-homophilous graphs. In Eq. (1), probabilities $p_\theta(k|\mathbf{v}_i)$ and $p_\theta(\mathbf{z}_j|\mathbf{v}_i, k)$ are not specified, and involve latent variables. To make it solvable, we introduce the following generative process.

Let $\boldsymbol{\mu}_k$ and $\boldsymbol{\Sigma}_k$ be the mean and variance of the latent mixture component k , and π_k be its corresponding mixture probability. The generation of a node and its neighbor typically involves three steps: (1) draw a latent variable k from a categorical distribution $p(k)$ on all mixture components, where $p(k)$ is usually defined as uniform distribution $p(k) = \frac{1}{K}$ for unknown graphs and better generalization, (2) draw the central node representation \mathbf{v}_i from the Gaussian distribution $p_\theta(\mathbf{v}_i|k) = \mathcal{N}(\mathbf{v}_i; \boldsymbol{\mu}_k, \boldsymbol{\Sigma}_k)$, and (3) draw the neighbor representation \mathbf{z}_j from Gaussian distribution $p_\theta(\mathbf{z}_j|\mathbf{v}_i, k) = \mathcal{N}(\mathbf{z}_j; \boldsymbol{\mu}_{z_j}, \boldsymbol{\Sigma}_j)$ where the mean depends both on central representation and latent variable: $\boldsymbol{\mu}_{z_j} = \mathbf{v}_i + g_\theta(k)$. Here the projector $g_\theta(\cdot)$ denotes another single fully connected network which embeds latent variable k (one-hot vector) to the representation space. In practice, to reduce complexity, we consider using isotropic Gaussian with tied variance, i.e., $\forall k : \boldsymbol{\Sigma}_k = \mathbf{I}\sigma_1^2$ and $\forall j : \boldsymbol{\Sigma}_j = \mathbf{I}\sigma_2^2$ where \mathbf{I} is the identity matrix, σ_1 and σ_2 are hyperparameters. In alignment with this generative process, the joint distribution of observed links and the latent variable can be written as:

$$p_\theta(\mathbf{v}_i, \mathbf{z}_j, k) = p_\theta(\mathbf{z}_j|\mathbf{v}_i, k) p_\theta(\mathbf{v}_i|k) p(k). \quad (2)$$

Intuitively, $p_\theta(\mathbf{v}_i|k)$ can be viewed as the probability for node representation under the k -th mixture component. Regarding $p_\theta(\mathbf{z}_j|\mathbf{v}_i, k) = \mathcal{N}(\mathbf{z}_j; \boldsymbol{\mu}_{z_j}, \boldsymbol{\Sigma}_j)$, this formulation is inspired from knowledge graph embedding [3], where two entities should be close to each other under a certain relation operation. However, unlike knowledge graph embedding, the relation context is latent variable and not observed in our unsupervised setting. Intuitively, instead of enforcing exact representation alignment of two linked nodes [24, 11, 14, 13, 40], our design can relax this exact homophily assumption and account for the semantic shift of representations between the central node and its neighbors via the inferred latent context k .

Now, the posterior probability $p_\theta(k|\mathbf{v}_i)$ in Eq. (1) can be derived by using Bayesian rules as follows:

$$p_\theta(k|\mathbf{v}_i) = \frac{p_\theta(\mathbf{v}_i|k)p(k)}{\sum_{k'=1}^K p_\theta(\mathbf{v}_i|k')p(k')} = \frac{\mathcal{N}(\mathbf{v}_i; \boldsymbol{\mu}_k, \mathbf{I}\sigma_1^2)p(k)}{\sum_{k'=1}^K \mathcal{N}(\mathbf{v}_i; \boldsymbol{\mu}_{k'}, \mathbf{I}\sigma_1^2)p(k')}, \quad (3)$$

where $\boldsymbol{\mu} = \{\boldsymbol{\mu}_k\}_{k=1}^K$ can be treated as a set of trainable prototype representations, which are the additional distribution parameters. This posterior probability represents the soft semantic assignment of the learned representation to the prototypes, which makes the node with similar semantic properties be close to its prototype and encode both the inter- and intra-cluster variation. Substituting $p_\theta(k|\mathbf{v}_i)$ and $p_\theta(\mathbf{z}_j|\mathbf{v}_i, k)$ in Eq. (1) with the specified probabilities, we get final objective $\mathcal{L}_{DSSL}(\theta, \boldsymbol{\mu})$.

3.3 Evidence Lower Bound

Given the framework above, we are interested in: (i) learning the model parameters θ and $\boldsymbol{\mu}$ by maximizing the log-likelihood $\mathcal{L}_{DSSL}(\theta, \boldsymbol{\mu})$, and (ii) inferring the posterior of latent variable k for each observed links. However, it is computationally intractable to directly solve these two problems due to the latent variables. To solve this, we resort to amortized variational inference methods [23], and maximize the evidence lower-bound (ELBO) of Eq. (1), i.e., $\mathcal{L}_{DSSL}(\theta, \boldsymbol{\mu}) \geq \mathcal{L}_{DSSL}(\theta, \phi, \boldsymbol{\mu})$:

$$\mathcal{L}(\theta, \phi, \boldsymbol{\mu}) = \frac{1}{|N(i)|} \sum_{j \in N(i)} \mathbb{E}_{q_\phi(k|\mathbf{v}_i, \mathbf{z}_j)} [\log p_\theta(\mathbf{z}_j|\mathbf{v}_i, k) + \log p_\theta(k|\mathbf{v}_i)] + \mathcal{H}(q_\phi(k|\mathbf{v}_i, \mathbf{z}_j)), \quad (4)$$

where $q_\phi(k|\mathbf{v}_i, \mathbf{z}_j)$ is the introduced variational distribution parameterized by ϕ and $\mathcal{H}(\cdot)$ is the entropy operator. \mathbf{z}_j is included in this variational posterior so that the inference is also conditioned on the neighborhood information. We derive this ELBO in Appendix A.1. Maximizing this ELBO w.r.t. $\{\theta, \phi, \boldsymbol{\mu}\}$ is equivalent to (i) maximize $\mathcal{L}_{DSSL}(\theta, \boldsymbol{\mu})$ and to (ii) make variational $q_\phi(k|\mathbf{v}_i, \mathbf{z}_j)$ be close to true posterior. Plugging the parameterized probabilities into this ELBO, we obtain the following loss to minimize (see Appendix A.2):

$$\mathcal{L} = \frac{1}{|N(i)|} \sum_{j \in N(i)} \mathbb{E}_{q_\phi(k|\mathbf{v}_i, \mathbf{z}_j)} [\|\mathbf{v}_i + g_\theta(k) - \mathbf{z}_j\|_2^2] - \sigma_2^2 \mathbb{E}_{q_\phi(k|\mathbf{v}_i)} \left[\log \frac{\exp(\mathbf{v}_i^\top \cdot \boldsymbol{\mu}_k / \sigma_1^2)}{\sum_{k'=1}^K \exp(\mathbf{v}_i^\top \cdot \boldsymbol{\mu}_{k'} / \sigma_1^2)} \right] - \mathcal{H}(q_\phi(k|\mathbf{v}_i, \mathbf{z}_j)), \quad (5)$$

where $q_\phi(k|\mathbf{v}_i) = 1/|N(i)| \sum_{j \in N(i)} q_\phi(k|\mathbf{v}_i, \mathbf{z}_j)$ is the posterior probability of semantic assignment for central node v_i , by aggregating all its neighbors. Thus, the first term (denoted as \mathcal{L}_{local}) in the loss encourages the model to reconstruct the local neighbors while considering different semantic shifts captured by latent variable k (see Figure 2 (b)). The second term (denoted as \mathcal{L}_{global}) encourages the model to perform clustering with learned representation where possible, i.e., seeking to push the representation \mathbf{v}_i to its closest prototype cluster (see Figure 2 (c)). The final entropy term makes the model choose to have high entropy over $q_\phi(k|\mathbf{v}_i, \mathbf{z}_j)$ such that all of the K -channel losses must be low. Overall, this loss can capture global semantic similarities over neighborhoods and learn to decouple different latent patterns in the local neighbors.

Regarding the variational distribution $q_\phi(k|\mathbf{v}_i, \mathbf{z}_j)$, we model it as categorical distribution since k is a discrete multinomial variable. Specifically, the representations \mathbf{v}_i and \mathbf{z}_j are encoded to a combined representation and then $q_\phi(k|\mathbf{v}_i, \mathbf{z}_j)$ is determined by an output softmax inference head as follows:

$$q_\phi(k|\mathbf{v}_i, \mathbf{z}_j) = \frac{\exp(h_\phi([\mathbf{v}_i; \mathbf{z}_j])[k])}{\sum_{k'=1}^K \exp(h_\phi([\mathbf{v}_i; \mathbf{z}_j])[k'])}, \quad (6)$$

where h_ϕ denotes the inference predictor network parameterized by ϕ and $[\cdot, \cdot]$ denotes the concatenation operation. $h_\phi([\mathbf{v}_i; \mathbf{z}_j])[k]$ indicates the k^{th} element, i.e., the logit corresponding the latent context k . Instead of introducing variational parameters individually, we consider the amortization inference, which fits a shared network to calculate each local parameter and is more efficient.

For the expectation terms in Eq. (5), back-propagation through the discrete variable k is not directly feasible. We alleviate this by adopting the Gumbel-Softmax estimator [18], which provides a continuous differentiable approximation for drawing samples from a categorical distribution. Specifically, for each sample, a latent cluster vector $\mathbf{c} \in (0, 1)^K$ is drawn from a reparameterization distribution:

$$\mathbf{c}[k] = \frac{\exp((h_\phi([\mathbf{v}_i; \mathbf{z}_j])[k] + \epsilon[k])/\gamma)}{\sum_{k'=1}^K \exp((h_\phi([\mathbf{v}_i; \mathbf{z}_j])[k'] + \epsilon[k'])/\gamma)}, \quad (7)$$

where $\epsilon[k]$ is i.i.d drawn from the Gumbel(0, 1) distribution and γ is a temperature. With this reparameterization trick, we can obtain the surrogate $\mathbb{E}_{q_\phi(k|\mathbf{v}_i, \mathbf{z}_j)} [\|\mathbf{v}_i + g_\theta(k) - \mathbf{z}_j\|_2^2] \simeq \mathbb{E}_\epsilon [\|\mathbf{v}_i + g_\theta(\mathbf{c}) - \mathbf{z}_j\|_2^2]$ and the gradients are estimated with Monte Carlo. The expectation term over $q_\phi(k|\mathbf{v}_i)$ can be similarly estimated. Thus, $\{\theta, \phi, \boldsymbol{\mu}\}$ in Eq. (5) can be efficiently solved by gradient descent.

3.4 Algorithm Optimization

The overall optimization steps involves simultaneously training (1) the encoder f_θ , (2) the projector g_θ , (3) the inference predictor h_ϕ and (4) the prototype vectors $\boldsymbol{\mu}$. The most canonical way to update the parameters is gradient descent. However, we observe that stochastically updating all parameters suffers from two problems: (1) Since we do not rely on negative samples, the objective admits trivial solutions, e.g., outputting the same representation for all nodes. (2) Updating prototypes without any constraints will lead to a degenerate solution, i.e., all nodes are assigned to a single cluster.

To address the issue of trivial solutions, inspired by the recent works [16, 10], we consider an asymmetric encoder architecture which includes online and target encoders. Specifically, for each node pair (v_i, v_j) , the online encoder f_θ produces the representation of the central node \mathbf{v}_i ; while the target encoder f_ξ is used to produce the representation of its neighbor \mathbf{z}_j . Importantly, the gradient of loss is only used to update the online encoder f_θ , while being blocked in the target encoder. The weights of the target encoder ξ are instead undated via exponential moving average of online encoder:

$$[\theta, \phi, \boldsymbol{\mu}] \leftarrow [\theta, \phi, \boldsymbol{\mu}] - \Gamma(\nabla_{\theta, \phi, \boldsymbol{\mu}} \mathcal{L}), \quad \xi \leftarrow \tau \xi + (1 - \tau)\theta, \quad (8)$$

where $\Gamma(\cdot)$ indicates a stochastic optimizer and $\tau \in [0, 1]$ is the target decay rate. This update introduces an asymmetry between two encoders that prevents collapse to trivial solutions [10, 41]. To alleviate the second issue, besides the stochastic update, we also apply an analytical global update for the prototype vectors $\boldsymbol{\mu} = \{\boldsymbol{\mu}_i\}_{i=1}^K$ at the end of each training epoch to avoid a degenerate solution:

$$\boldsymbol{\mu}_k = \frac{\sum_{i=1}^N \pi_i(k) \cdot \mathbf{v}_i}{\|\sum_{i=1}^N \pi_i(k) \cdot \mathbf{v}_i\|_2}, \quad \text{where } \pi_i(k) = 1/|N(i)| \sum_{j \in N(i)} q_\phi(k|\mathbf{v}_i, \mathbf{z}_j). \quad (9)$$

The detailed derivation is provided in Appendix A.3. Intuitively, $\pi_i(k)$ reflects the degree of relevance of node v_i to the k^{th} prototype. Instead of only updating the prototypes in a mini-batch, we also aggregate all the representation as the prototype based on the soft assignment probability.

After the training is finished, we only keep the online encoder f_θ for the downstream task. Our full algorithm and network are provided in Appendix B. The time complexity of DSSL is $O(N \cdot d)$ where d is the average node degree. Note that we omit the complexity introduced by the GNN encoder and dot-product computation, as it is orthogonal to the SSL design. Compared to the recent SSL approaches [33, 46, 59, 53, 15] which requires computation and memory quadratic in the number of nodes, our method scales linearly in the size of nodes, thus is trained in a more efficient way.

3.5 Theoretical Analysis

In this section, we provide theoretical analysis of the proposed framework. We first present the connection between the proposed objective and the mutual information maximization, then show that the learned representations by our objective provably enjoy good downstream performance. Due to the space limitation, all proofs of theorems and corollaries are provided in Appendix C.

We denote the random variable of the input graph as \mathbf{g} and the downstream label as \mathbf{y} . For clarity, we omit subscript i in what follows. Note that downstream tasks could be the node classification or clustering. From an information-theoretic learning perspective, a desirable way is to maximize the mutual information $I(\mathbf{v}, \mathbf{y})$ between the node representation \mathbf{v} and its downstream label \mathbf{y} . However, due to the lack of the downstream label, self-supervised learning resorts to maximizing $I(\mathbf{v}, \mathbf{s})$ where \mathbf{s} is the designed self-supervised signal for different methods [44, 4, 55, 8]. In our method, we actually has two self-supervised signal: the global semantic cluster information inferred by k and the local structural roles captured by the representations of the neighbors $\mathbf{z} = \{\mathbf{z}_i | v_i \in N(v)\}$ of node v .

Then, we can interpret our objective in Eq. (5) from the information maximization perspective:

Theorem 1. *Optimizing Eq. (5) is equivalent to maximize the mutual information between the node representation \mathbf{v} and the global semantic signal k , and maximize the conditional mutual information between \mathbf{v} and the local signal \mathbf{z} , conditioned on the global signal k . Formally, we have :*

$$\max_{\theta, \phi, \boldsymbol{\mu}} \mathcal{L} \Rightarrow \max_{\mathbf{v}} I(\mathbf{v}; k) + I(\mathbf{v}; \mathbf{z}|k) = I(\mathbf{v}; k, \mathbf{z}). \quad (10)$$

This theorem suggests that we essentially combine both local structure and global semantic information as the self-supervised signal and maximize the mutual information between the representation \mathbf{v} and their joint distribution (k, \mathbf{z}) . Next, we discuss how the learned representation affect the downstream task \mathbf{y} based on the information bottleneck principle [44, 8, 4]. The rationality of self-supervised learning is that the task-relevant information lies mostly in the shared information between the input and the self-supervised signals [44, 8, 4]. Specifically, we formulate our lightweight and reasonable assumption below, which serves as a foundation for our analysis.

Assumption 1. *Nodes with similar labels should have similar “local structural roles” and “global semantic clusters”. In this work, we equate “local structure” with the 1-hop neighborhood and “global semantic” with the clustering membership of a node. Formally, we have the task-relevant information \mathbf{y} left in \mathbf{g} except that in joint self-supervised signal (\mathbf{z}, k) is relatively small: $I(\mathbf{g}; \mathbf{y}|\mathbf{z}, k) \leq \epsilon$.*

Intuitively, this assumption indicates that most of the task-relevant information in the graph is contained in the self-supervised signal. Based on this assumption, we give the following theorem which reveals that why the downstream tasks can benefit from the learned representations learned.

Theorem 2. Let $\mathbf{v}_{\text{joint}} = \arg \max_{\mathbf{v}} I(\mathbf{v}; \mathbf{z}, k)$, $\mathbf{v}_{\text{local}} = \arg \max_{\mathbf{v}} I(\mathbf{v}; k)$, and $\mathbf{v}_{\text{global}} = \arg \max_{\mathbf{v}} I(\mathbf{v}; \mathbf{z})$. Formally, we have the following inequalities about the task-relevant information:

$$I(\mathbf{g}; \mathbf{y}) = \max_{\mathbf{v}} I(\mathbf{v}; \mathbf{y}) \geq I(\mathbf{v}_{\text{joint}}; \mathbf{y}) \geq \max(I(\mathbf{v}_{\text{local}}; \mathbf{y}), I(\mathbf{v}_{\text{global}}; \mathbf{y})) \geq I(\mathbf{g}; \mathbf{y}) - \epsilon. \quad (11)$$

Theorem 2 shows that the gap of task-relevant information between supervised representation $\mathbf{v}_{\text{sup}} = \arg \max_{\mathbf{v}} I(\mathbf{v}; \mathbf{y})$ and self-supervised representation $\mathbf{v}_{\text{joint}}$ is ϵ . Thus, we can guarantee a good downstream performance as long as the Assumption 1 is satisfied. It is noteworthy that jointly utilizing local structure and global semantic as the self-supervised signal is expected to contain more task information. As further enlightenment, we can relate Eq. (38) with the Bayes error rate [44]:

Corollary 1. Suppose that downstream label \mathbf{y} is a M -categorical random variable. Then we have the upper bound for the downstream Bayes errors $P_{\mathbf{v}}^e = \mathbb{E}_{\mathbf{v}} [1 - \max_{y \in \mathbf{y}} P(\hat{\mathbf{y}} = y | \mathbf{v})]$ on learned representation \mathbf{v} , where $\hat{\mathbf{y}}$ is the estimation for label from our downstream classifier:

$$\text{Th}(P_{\mathbf{v}_{\text{joint}}}^e) \leq \log 2 + P_{\mathbf{v}_{\text{sup}}}^e \cdot \log M + I(\mathbf{g}; \mathbf{y} | \mathbf{z}, k) \triangleq \text{RHS}_{\mathbf{v}_{\text{joint}}} \quad (12)$$

where $\text{Th}(x) = \min\{\max\{x, 0\}, 1 - 1/|M|\}$ is a thresholded operation [44]. Similarly, we can obtain the error upper bound of other representations $\mathbf{v}_{\text{local}}$ and $\mathbf{v}_{\text{global}}$: $\text{RHS}_{\mathbf{v}_{\text{local}}}$ and $\text{RHS}_{\mathbf{v}_{\text{global}}}$. Then, we have inequalities on error upper bounds: $\text{RHS}_{\mathbf{v}_{\text{joint}}} \leq \min(\text{RHS}_{\mathbf{v}_{\text{local}}}, \text{RHS}_{\mathbf{v}_{\text{global}}})$.

This corollary says that our self-supervised signal has a tighter upper bound on the downstream Bayes error. Thus, we can expect that the representation learned by our objective function which utilizes both local structure and global semantic information have superior performance on downstream tasks.

4 Experiments

In this section, we empirically evaluate the proposed self-supervised learning method on real-world datasets, and analyze its behavior on graphs to gain further insights. We include additional experiments in Appendix E.

4.1 Experimental Setup

Datasets. We perform experiments on widely-used homophilic graph datasets: Cora, Citeseer, and Pubmed [38], as well as non-homophilic datasets: Texas, Cornell, Wisconsin [32], Penn94 and Twitch. Penn94 and Twitch are two relatively large non-homophilous graph datasets proposed by [37, 27]. We provide the detailed descriptions, statistics and homophily measures of datasets in Appendix D.1.

Baselines. To evaluate the effectiveness of our proposed DSSL, we consider the following representative unsupervised and self-supervised learning methods for the node representation task, including Deepwalk [34], LINE [40], Struc2vec [36], GAE [24], VGAE [24], DGI [46], GraphCL [53], MVGRL [15] and BGRL [41]. The detailed description of baselines and implementations are given in Appendix D.2.

Evaluation Protocol. We consider two types of downstream tasks: node classification and node clustering. For node classification, we follow the standard linear-evaluation protocol on graphs [46, 41], where a linear classifier is trained on top of the frozen representation, and test accuracy (ACC) is used as a proxy for representation quality. For all datasets, we adopt the same random split with train/val/test split ratio of 60%/20%/20% for the training of downstream linear classifier [27]. For the node clustering task, we perform K -means clustering on the obtained representations and set the number of clusters to the number of classes. We utilize the normalized mutual information (NMI) [47] as the evaluation metric for clustering.

Setup. For all self-supervised methods, we consider a two-layer GCN [25] as the encoder and randomly initialize parameters. We also test methods with other encoders such as GAT [45] (see Appendix E.1). we run experiments with 10 random splits and report the average performance. We select the best configuration of hyper-parameters based on accuracy on the validation. The detailed settings are given in Appendix D.3.

4.2 Overall Performance Comparison

In this section, we conduct experiments on real-world graphs compared to state-of-the-art methods. Table 1 reports the average classification accuracy with the standard deviation on node classification after 10 runs. Since node clustering results have a similar tendency, we provide them in Appendix E.2. From Table 1,

Table 1: Experimental results (%) with standard deviations on the node classification task. The best and second best performance under each dataset are marked with blue and underline, respectively.

Method	Cora	Citeseer	Pubmed	Texas	Cornell	Squirrel	Penn94	Twitch
Deepwalk	77.14±0.82	67.85±0.79	79.38±1.22	42.31±2.21	41.55±3.12	37.54±2.19	56.13±0.46	66.37±0.11
LINE	78.93±0.55	68.79±0.41	80.56±0.92	48.69±1.39	43.68±2.17	<u>38.92±1.58</u>	57.59±0.17	67.23±0.27
Struc2vec	30.26±1.52	53.38±0.62	40.83±1.85	49.31±3.22	30.22±5.87	36.49±1.15	50.29±0.31	63.52±0.35
GAE	78.33±0.27	66.39±0.24	78.28±0.77	53.98±3.22	44.18±3.56	30.53±1.33	58.11±0.18	67.98±0.27
VGAE	80.59±0.35	69.90±0.57	81.33±0.69	50.27±2.21	48.73±4.19	29.13±1.16	58.29±0.21	65.09±0.08
DGI	84.17±1.35	71.80±1.33	81.65±0.71	<u>58.53±2.98</u>	45.33±6.11	26.44±1.12	53.68±0.19	66.97±0.25
GraphCL	84.28±0.91	72.46±1.79	81.96±0.73	48.67±4.37	47.22±4.50	22.53±0.98	58.43±0.31	68.37±0.16
MVGRL	85.21±1.18	72.13±1.04	82.33±0.88	51.26±0.38	<u>51.16±1.67</u>	38.43±0.87	57.22±0.17	66.03±0.26
BGRL	83.29±0.72	71.56±0.87	81.34±0.50	52.77±1.98	50.33±2.29	36.22±1.97	<u>58.98±0.13</u>	67.43±0.22
DSSL	83.06±0.53	73.51±0.64	82.98±0.49	62.11±1.53	53.15±1.28	40.51±0.38	60.38±0.32	69.81±0.17

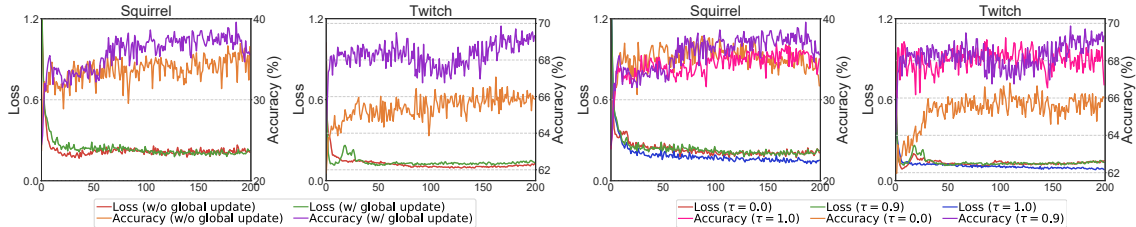


Figure 3: (Left) Performance w and w/o global update on prototypes. (Right) Performance with varying τ .

we have the following observations: (1) Generally, our DSSL achieves the best performance on both node clustering and classification tasks over the best baseline, demonstrating the effectiveness of DSSL on both homophilous and non-homophilous graphs and the robustness to different downstream tasks and graphs. Especially, DSSL achieves an relative improvement of over 6% and 4% on Texas and Squirrel compared to the best baselines (2) Our DSSL cannot achieve the best performance on Cora. This is reasonable since Cora is highly homophilous (see Appendix D.1), and the core design of augmentation in contrastive learning methods such as MVGRL and GraphCL enables them to be effective on homophilous graphs but failed on low-homophily settings. This supports our motivation in the introduction that it is relatively difficult to design effective graph augmentation on non-homophilous graphs due to their heterogeneous and diverse patterns. (3) When compared with GAE, VGAE, and DGI, DSSL consistently and significantly outperforms them. We deem that this improvement is mainly from the joint local semantic shift and global semantic clustering in DSSL, which is not included in existing methods.

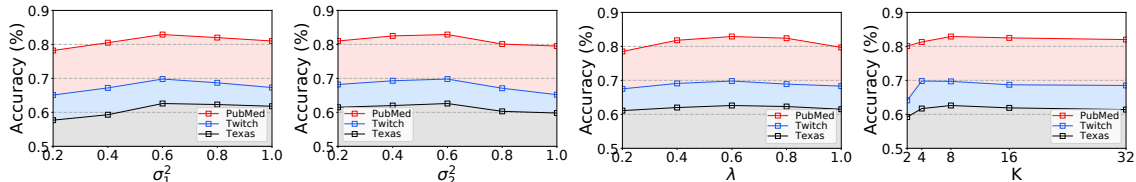


Figure 4: Hyper-parameter analysis on PubMed, Twitch and Texas. We provide results on other datasets in Appendix E.3

4.3 Ablation Study and Parameter Analysis

In this section, we conduct an ablation study to validate our motivation and design, and investigate the sensitivity of hyper-parameters. We refer readers to Appendix E.3 for more results.

Ablation Study. We consider the following ablations: (A1) We remove the key component of DSSL: the local reconstruction loss (w/o \mathcal{L}_{local}). (A2) We remove global clustering loss to see if \mathcal{L}_{local} alone is still effective (w/o \mathcal{L}_{global}). (A3) We remove the entropy term in Eq. (5) (w/o entropy). (A4) We remove the semantic shift term $g_\theta(k)$ in \mathcal{L}_{local} (w/o semantic shift). (A5) We set posterior $q_\phi(k|\mathbf{v}_i, \mathbf{z}_j) = 1/K$ as uniform distribution for each link (w/ uniform posterior). We show the ablation study results in Table 2. \mathcal{L}_{global} alone does not provide many discriminative information and it does not perform very well. \mathcal{L}_{local} as a key component of DSSL alone produces better results than the baselines. We also observe that considering semantic shift and personalized posterior can improve the performance a lot which demonstrates our key motivations. The full model (last row) achieves the best performance, which illustrates that different components designed are complementary to each other.

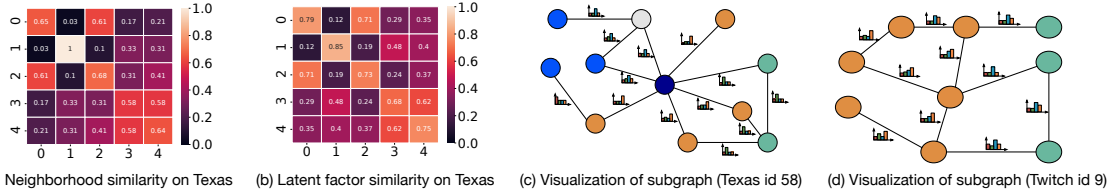


Figure 5: The visualization and case study results (best viewed on a computer screen and note that the latent distribution of each link need to be zoomed in to be better visible). More results can be found in Appendix E.4.

Effect of Global Update on Prototypes. We also conduct the ablation studies to gain insights into the global update on prototypes. As shown in Figure 3, we can observe that without Eq. (9), the performance is not very good and we are stuck in bad local optima. As discussed in previous sections, a possible reason is that we will experience strong degeneracy if we only update prototype vectors with mini-batch training. This figure also demonstrates that DSSL can converge within a few hundred steps, which is efficient.

Effect of Asymmetric Architecture. We then explore the effect of target decay rate τ on the performance. Figure 3 shows the learning curves of DSSL on Squirrel and Twitch. We can observe that the best result is achieved at $\tau = 0.9$. When $\tau = 1.0$, i.e., the target network is never updated, DSSL obtains a competitive result but is lower than $\tau = 0.9$. This confirms that slowly updating the target network is crucial in obtaining superior performance. At the other extreme value $\tau = 0$, the target network is the same as online network and DSSL demonstrates a degenerated performance and severe overfitting phenomena on Squirrel.

Hyper-parameters Analysis. We investigate the hyper-parameters most essential to our framework design, i.e., the standard deviation σ_1 and σ_2 , the temperature of the Gumbel Softmax γ , and the total number of factors K . The corresponding results are shown in Figure 4. σ_1^2 resembles the temperature scaling in Eq. (5). We observe σ_1^2 is better to be selected from 0.6 to 1.0, and a too small (e.g., 0.2) value may degenerate the performance in the all three datasets. σ_2^2 balances the local and global loss in Eq. (5). We can find that having large values of σ_2^2 does not improve the performance, as the local loss plays more essential role in the proposed model. Further, we observe that DSSL is not very sensitive to the Gumbel softmax temperature λ , while a moderate hardness of the Softmax gives the best results. We also find that as K increases from 2 to 8, the performance of DGCL improves, which suggests the importance of decoupling latent factors. However, training with large K will lead performance slightly drop due to the introduced high model complexity.

4.4 Visualization and Case Study

In this section, to understand how DSSL uncovers the latent patterns in neighborhoods, we provide the visualization and case study results. In Figure 5 (a), we first calculate the cross-class neighborhood similarity (see Appendix E.4 for definition), which serves as the ground truth. If nodes with the same label share the same neighborhood distributions, the intra-class similarity should be high. In Figure 5 (b), we calculate average posterior distribution $q_\phi(k|\mathbf{v}_i)$ over all nodes on each class and provide cosine similarity of them. We can observe that our learned latent factor distribution shares a similar pattern with the cross-class neighborhood similarity, which meets our expectation that the latent factors can capture the latent semantic information related to neighborhood patterns. To evaluate if DSSL can learn the semantic shift of between different neighbors, we plot the latent factor, i.e., $q_\phi(k|\mathbf{v}_i, \mathbf{z}_j)$ for individual links. In Figures 5 (b) and (c), we plot the subgraph of a randomly selected node, and the distribution $q_\phi(k|\mathbf{v}_i, \mathbf{z}_j)$ ($K=4$) and use different colors to indicate different labels. We find that similar neighbors over class generally have a similar distribution, while different types of links exhibit different latent distributions. This observation matches our motivation that our latent factors can decouple the diverse semantics in the local neighborhoods.

5 Conclusions

In this paper, we study the problem of learning unsupervised node representations on non-homophilous graphs data. We present a novel decoupled self-supervised learning (DSSL) framework to decouple the diverse neighborhood context of a node in an unsupervised manner. Specifically, DSSL imitates the generative

Table 2: Node classification accuracy (%) on the Texas dataset. Ablation results for other datasets are given in Appendix E.3.

Ablation	Accuracy
A1 w/o local loss \mathcal{L}_{local}	25.18 \pm 1.31
A2 w/o global loss \mathcal{L}_{global}	59.34 \pm 2.76
A3 w/o entropy loss	60.57 \pm 1.27
A4 w/o semantic shift	56.19 \pm 1.25
A5 w/ uniform posterior	50.27 \pm 1.04
A2+A3	57.61 \pm 1.72
A2+A4	50.52 \pm 2.01
A2+A5	48.59 \pm 1.87
DGI	58.53 \pm 2.98
DSSL	62.11\pm1.53

process of neighbors and explicitly models unobserved factors by latent variables. We show that DSSL can simultaneously capture the global clustering information and the local structure roles with the semantic shift. We theoretically show that DSSL enjoys a good downstream performance. Extensive experiments on several graph benchmarks showed that DSSL could learn meaningful class-discriminative representations.

References

- [1] Kristen M Altenburger and Johan Ugander. Monophily in social networks introduces similarity among friends-of-friends. *Nature human behaviour*, pages 284–290, 2018.
- [2] Deyu Bo, Xiao Wang, Chuan Shi, and Huawei Shen. Beyond low-frequency information in graph convolutional networks. In *Proceedings of the AAAI Conference on Artificial Intelligence*, pages 3950–3957, 2021.
- [3] Antoine Bordes, Nicolas Usunier, Alberto Garcia-Duran, Jason Weston, and Oksana Yakhnenko. Translating embeddings for modeling multi-relational data. *Advances in neural information processing systems*, 2013.
- [4] Manh-Ha Bui, Toan Tran, Anh Tran, and Dinh Phung. Exploiting domain-specific features to enhance domain generalization. *Advances in Neural Information Processing Systems*, 2021.
- [5] Ming Chen, Zhewei Wei, Zengfeng Huang, Bolin Ding, and Yaliang Li. Simple and deep graph convolutional networks. In *International Conference on Machine Learning*, pages 1725–1735, 2020.
- [6] Eli Chien, Jianhao Peng, Pan Li, and Olgica Milenkovic. Adaptive universal generalized pagerank graph neural network. In *International Conference on Learning Representations*, 2020.
- [7] Linus Ericsson, Henry Gouk, and Timothy M Hospedales. How well do self-supervised models transfer? In *Proceedings of the IEEE/CVF Conference on Computer Vision and Pattern Recognition*, pages 5414–5423, 2021.
- [8] Marco Federici, Anjan Dutta, Patrick Forré, Nate Kushman, and Zeynep Akata. Learning robust representations via multi-view information bottleneck. In *International Conference on Learning Representations*, 2019.
- [9] Spyros Gidaris, Praveer Singh, and Nikos Komodakis. Unsupervised representation learning by predicting image rotations. In *International Conference on Learning Representations*, 2018.
- [10] Jean-Bastien Grill, Florian Strub, Florent Altché, Corentin Tallec, Pierre Richemond, Elena Buchatskaya, Carl Doersch, Bernardo Avila Pires, Zhaohan Guo, Mohammad Gheshlaghi Azar, et al. Bootstrap your own latent—a new approach to self-supervised learning. *Advances in Neural Information Processing Systems*, pages 21271–21284, 2020.
- [11] Aditya Grover and Jure Leskovec. node2vec: Scalable feature learning for networks. In *Proceedings of the 22nd ACM SIGKDD international conference on Knowledge discovery and data mining*, pages 855–864, 2016.
- [12] Aditya Grover, Aaron Zweig, and Stefano Ermon. Graphite: Iterative generative modeling of graphs. In *International conference on machine learning*, pages 2434–2444, 2019.
- [13] William L Hamilton, Rex Ying, and Jure Leskovec. Inductive representation learning on large graphs. In *NeurIPS*, 2017.
- [14] William L Hamilton, Rex Ying, and Jure Leskovec. Representation learning on graphs: Methods and applications. *arXiv preprint arXiv:1709.05584*, 2017.
- [15] Kaveh Hassani and Amir Hosein Khasahmadi. Contrastive multi-view representation learning on graphs. In *International Conference on Machine Learning*, pages 4116–4126, 2020.
- [16] Kaiming He, Haoqi Fan, Yuxin Wu, Saining Xie, and Ross Girshick. Momentum contrast for unsupervised visual representation learning. In *Proceedings of the IEEE/CVF conference on computer vision and pattern recognition*, pages 9729–9738, 2020.

- [17] W Hu, B Liu, J Gomes, M Zitnik, P Liang, V Pande, and J Leskovec. Strategies for pre-training graph neural networks. In *International Conference on Learning Representations (ICLR)*, 2020.
- [18] Eric Jang, Shixiang Gu, and Ben Poole. Categorical reparameterization with gumbel-softmax. *arXiv preprint arXiv:1611.01144*, 2016.
- [19] Di Jin, Zhizhi Yu, Cuiying Huo, Rui Wang, Xiao Wang, Dongxiao He, and Jiawei Han. Universal graph convolutional networks. *Advances in Neural Information Processing Systems*, 2021.
- [20] Wei Jin, Tyler Derr, Haochen Liu, Yiqi Wang, Suhang Wang, Zitao Liu, and Jiliang Tang. Self-supervised learning on graphs: Deep insights and new direction. *arXiv preprint arXiv:2006.10141*, 2020.
- [21] Wei Jin, Tyler Derr, Yiqi Wang, Yao Ma, Zitao Liu, and Jiliang Tang. Node similarity preserving graph convolutional networks. In *Proceedings of the 14th ACM International Conference on Web Search and Data Mining*, pages 148–156, 2021.
- [22] Diederik P Kingma and Jimmy Ba. Adam: A method for stochastic optimization. *arXiv preprint arXiv:1412.6980*, 2014.
- [23] Diederik P. Kingma and Max Welling. Auto-encoding variational bayes. In *International Conference on Learning Representations*, 2014.
- [24] Thomas N Kipf and Max Welling. Variational graph auto-encoders. *arXiv preprint arXiv:1611.07308*, 2016.
- [25] Thomas N. Kipf and Max Welling. Semi-supervised classification with graph convolutional networks. In *ICLR*, 2017.
- [26] Haoyang Li, Xin Wang, Ziwei Zhang, Zehuan Yuan, Hang Li, and Wenwu Zhu. Disentangled contrastive learning on graphs. *Advances in Neural Information Processing Systems*, 2021.
- [27] Derek Lim, Felix Hohne, Xiuyu Li, Sijia Linda Huang, Vaishnavi Gupta, Omkar Bhalerao, and Ser Nam Lim. Large scale learning on non-homophilous graphs: New benchmarks and strong simple methods. *Advances in Neural Information Processing Systems*, 34, 2021.
- [28] Derek Lim, Xiuyu Li, Felix Hohne, and Ser-Nam Lim. New benchmarks for learning on non-homophilous graphs. *arXiv preprint arXiv:2104.01404*, 2021.
- [29] Yanbei Liu, Xiao Wang, Shu Wu, and Zhitao Xiao. Independence promoted graph disentangled networks. In *Proceedings of the AAAI Conference on Artificial Intelligence*, pages 4916–4923, 2020.
- [30] Jianxin Ma, Peng Cui, Kun Kuang, Xin Wang, and Wenwu Zhu. Disentangled graph convolutional networks. In *International conference on machine learning*, pages 4212–4221, 2019.
- [31] Shashank Pandit, Duen Horng Chau, Samuel Wang, and Christos Faloutsos. Netprobe: a fast and scalable system for fraud detection in online auction networks. In *Proceedings of the 16th international conference on World Wide Web*, pages 201–210, 2007.
- [32] Hongbin Pei, Bingzhe Wei, Kevin Chen-Chuan Chang, Yu Lei, and Bo Yang. Geom-gcn: Geometric graph convolutional networks. In *International Conference on Learning Representations*, 2019.
- [33] Zhen Peng, Wenbing Huang, Minnan Luo, Qinghua Zheng, Yu Rong, Tingyang Xu, and Junzhou Huang. Graph representation learning via graphical mutual information maximization. In *Proceedings of The Web Conference 2020*, 2020.
- [34] Bryan Perozzi, Rami Al-Rfou, and Steven Skiena. Deepwalk: Online learning of social representations. In *Proceedings of the 20th ACM SIGKDD international conference on Knowledge discovery and data mining*, pages 701–710, 2014.
- [35] Ben Poole, Sherjil Ozair, Aaron Van Den Oord, Alex Alemi, and George Tucker. On variational bounds of mutual information. In *International Conference on Machine Learning*, pages 5171–5180, 2019.

- [36] Leonardo FR Ribeiro, Pedro HP Saverese, and Daniel R Figueiredo. struc2vec: Learning node representations from structural identity. In *Proceedings of the 23rd ACM SIGKDD international conference on knowledge discovery and data mining*, pages 385–394, 2017.
- [37] Benedek Rozemberczki, Carl Allen, and Rik Sarkar. Multi-scale attributed node embedding. *Journal of Complex Networks*, page cnab014, 2021.
- [38] Prithviraj Sen, Galileo Namata, Mustafa Bilgic, Lise Getoor, Brian Galligher, and Tina Eliassi-Rad. Collective classification in network data. *AI magazine*, pages 93–93, 2008.
- [39] Susheel Suresh, Pan Li, Cong Hao, and Jennifer Neville. Adversarial graph augmentation to improve graph contrastive learning. *Advances in Neural Information Processing Systems*, 2021.
- [40] Jian Tang, Meng Qu, Mingzhe Wang, Ming Zhang, Jun Yan, and Qiaozhu Mei. Line: Large-scale information network embedding. In *Proceedings of the 24th international conference on world wide web*, pages 1067–1077, 2015.
- [41] Shantanu Thakoor, Corentin Tallec, Mohammad Gheshlaghi Azar, Mehdi Azabou, Eva L Dyer, Remi Munos, Petar Veličković, and Michal Valko. Large-scale representation learning on graphs via bootstrapping. In *International Conference on Learning Representations*, 2021.
- [42] MTCAJ Thomas and A Thomas Joy. *Elements of information theory*. Wiley-Interscience, 2006.
- [43] Puja Trivedi, Ekdeep Singh Lubana, Yujun Yan, Yaoqing Yang, and Danai Koutra. Augmentations in graph contrastive learning: Current methodological flaws & towards better practices. *arXiv preprint arXiv:2111.03220*, 2021.
- [44] Yao-Hung Hubert Tsai, Yue Wu, Ruslan Salakhutdinov, and Louis-Philippe Morency. Demystifying self-supervised learning: An information-theoretical framework. *arXiv preprint arXiv:2006.05576*, 2020.
- [45] Petar Velickovic, Guillem Cucurull, Arantxa Casanova, Adriana Romero, Pietro Liò, and Yoshua Bengio. Graph attention networks. In *ICLR*, 2018.
- [46] Petar Veličković, William Fedus, William L Hamilton, Pietro Liò, Yoshua Bengio, and R Devon Hjelm. Deep graph infomax. In *International Conference on Learning Representations*, 2018.
- [47] Nguyen Xuan Vinh, Julien Epps, and James Bailey. Information theoretic measures for clusterings comparison: Variants, properties, normalization and correction for chance. *The Journal of Machine Learning Research*, pages 2837–2854, 2010.
- [48] Zhirong Wu, Yuanjun Xiong, Stella X Yu, and Dahua Lin. Unsupervised feature learning via non-parametric instance discrimination. In *Proceedings of the IEEE conference on computer vision and pattern recognition*, pages 3733–3742, 2018.
- [49] Teng Xiao, Zhengyu Chen, Donglin Wang, and Suhang Wang. Learning how to propagate messages in graph neural networks. In *Proceedings of the 27th ACM SIGKDD Conference on Knowledge Discovery & Data Mining*, 2021.
- [50] Keyulu Xu, Chengtao Li, Yonglong Tian, Tomohiro Sonobe, Ken-ichi Kawarabayashi, and Stefanie Jegelka. Representation learning on graphs with jumping knowledge networks. In *ICML*, 2018.
- [51] Liang Yang, Mengzhe Li, Liyang Liu, Chuan Wang, Xiaochun Cao, Yuanfang Guo, et al. Diverse message passing for attribute with heterophily. *Advances in Neural Information Processing Systems*, 2021.
- [52] Yiding Yang, Zunlei Feng, Mingli Song, and Xinchao Wang. Factorizable graph convolutional networks. *Advances in Neural Information Processing Systems*, pages 20286–20296, 2020.
- [53] Yuning You, Tianlong Chen, Yongduo Sui, Ting Chen, Zhangyang Wang, and Yang Shen. Graph contrastive learning with augmentations. *Advances in Neural Information Processing Systems*, pages 5812–5823, 2020.

- [54] Yuning You, Tianlong Chen, Zhangyang Wang, and Yang Shen. When does self-supervision help graph convolutional networks? In *international conference on machine learning*, pages 10871–10880. PMLR, 2020.
- [55] Hengrui Zhang, Qitian Wu, Junchi Yan, David Wipf, and Philip S Yu. From canonical correlation analysis to self-supervised graph neural networks. *Advances in Neural Information Processing Systems*, 2021.
- [56] Tianxiang Zhao, Xiang Zhang, and Suhang Wang. Exploring edge disentanglement for node classification. *arXiv preprint arXiv:2202.11245*, 2022.
- [57] Jiong Zhu, Yujun Yan, Lingxiao Zhao, Mark Heimann, Leman Akoglu, and Danai Koutra. Beyond homophily in graph neural networks: Current limitations and effective designs. *Advances in Neural Information Processing Systems*, pages 7793–7804, 2020.
- [58] Yanqiao Zhu, Yichen Xu, Qiang Liu, and Shu Wu. An empirical study of graph contrastive learning. *arXiv preprint arXiv:2109.01116*, 2021.
- [59] Yanqiao Zhu, Yichen Xu, Feng Yu, Qiang Liu, Shu Wu, and Liang Wang. Graph contrastive learning with adaptive augmentation. In *Proceedings of the Web Conference 2021*, pages 2069–2080, 2021.
- [60] Marinka Zitnik, Rok Sosič, and Jure Leskovec. Prioritizing network communities. *Nature communications*, pages 1–9, 2018.

A The Omitted Derivations

A.1 The Evidence Lower-Bound

In this section, we provide the details of the lower-bound in Eq. (4). By introducing the approximated posterior $q_\phi(k|\mathbf{v}_i, \mathbf{z}_j)$, the likelihood $\mathcal{L}(\theta, \boldsymbol{\mu})$ in Eq. (2) becomes:

$$\begin{aligned}
\mathcal{L}(\theta, \boldsymbol{\mu}) &= \frac{1}{|N(i)|} \sum_{j \in N(i)} \log \left[\sum_{k=1}^K p_\theta(\mathbf{z}_j | \mathbf{v}_i, k) p_\theta(k | \mathbf{v}_i) \right] \\
&= \frac{1}{|N(i)|} \sum_{j \in N(i)} \log \left[\sum_{k=1}^K p_\theta(\mathbf{z}_j | \mathbf{v}_i, k) p_\theta(k | \mathbf{v}_i) \frac{q_\phi(k | \mathbf{v}_i, \mathbf{z}_j)}{q_\phi(k | \mathbf{v}_i, \mathbf{z}_j)} \right] \\
&\geq \frac{1}{|N(i)|} \sum_{j \in N(i)} \sum_{k=1}^K q_\phi(k | \mathbf{v}_i, \mathbf{z}_j) [\log p_\theta(\mathbf{z}_j | \mathbf{v}_i, k) + \log p_\theta(k | \mathbf{v}_i) - \log q_\phi(k | \mathbf{v}_i, \mathbf{z}_j)] \\
&= \frac{1}{|N(i)|} \sum_{j \in N(i)} \mathbb{E}_{q_\phi(k | \mathbf{v}_i, \mathbf{z}_j)} [\log p_\theta(\mathbf{z}_j | \mathbf{v}_i, k) + \log p_\theta(k | \mathbf{v}_i) - \log q_\phi(k | \mathbf{v}_i, \mathbf{z}_j)], \quad (13)
\end{aligned}$$

where the third step uses Jensen's inequality. This completes the derivation of Eq. (4).

A.2 The Optimization Loss

In this section, we derive the optimization loss for learning parameters in Eq. (5). Introducing the posterior in Eq. (3) and probabilities specification $p_\theta(\mathbf{z}_j | \mathbf{v}_i, k) = \mathcal{N}(\mathbf{z}_j; \boldsymbol{\mu}_{z_j}, \boldsymbol{\Sigma}_j)$ to the negative of the lower-bounded likelihood in Eq. (4), we have:

$$\begin{aligned}
\mathcal{L} &= -\frac{1}{|N(i)|} \sum_{j \in N(i)} \mathbb{E}_{q_\phi(k | \mathbf{v}_i, \mathbf{z}_j)} [\log \mathcal{N}(\mathbf{z}_j; \boldsymbol{\mu}_{z_j}, \boldsymbol{\Sigma}_j) + \log \frac{\mathcal{N}(\mathbf{v}_i; \boldsymbol{\mu}_k, \mathbf{I}\sigma_1^2) p(k)}{\sum_{k'=1}^K \mathcal{N}(\mathbf{v}_i; \boldsymbol{\mu}_{k'}, \mathbf{I}\sigma_1^2) p(k')} \\
&\quad - \log q_\phi(k | \mathbf{v}_i, \mathbf{z}_j)]. \quad (14)
\end{aligned}$$

Since we consider isotropic Gaussian with $\boldsymbol{\Sigma}_j = \mathbf{I}\sigma_2^2$, we have:

$$\begin{aligned}
\mathcal{N}(\mathbf{z}_j; \boldsymbol{\mu}_{z_j}, \boldsymbol{\Sigma}_j) &= \frac{1}{(2\pi)^{D'/2} \sigma_2^{D'}} \exp\left(-\frac{1}{2\sigma_2^2} (\mathbf{z}_j - \mathbf{v}_i - g_\theta(k))^T \cdot (\mathbf{z}_j - \mathbf{v}_i - g_\theta(k))\right) \\
&= \frac{1}{(2\pi)^{D'/2} \sigma_2^{D'}} \exp\left(-\frac{\|\mathbf{v}_i + g_\theta(k) - \mathbf{z}_j\|_2^2}{2\sigma_2^2}\right) \quad (15)
\end{aligned}$$

Similarly, for $\mathcal{N}(\mathbf{v}_i; \boldsymbol{\mu}_k, \mathbf{I}\sigma_1^2)$, we have:

$$\begin{aligned}
\mathcal{N}(\mathbf{v}_i; \boldsymbol{\mu}_k, \mathbf{I}\sigma_1^2) &= \frac{1}{(2\pi)^{D'/2} \sigma_1^{D'}} \exp\left(-\frac{1}{2\sigma_1^2} (\mathbf{v}_i - \boldsymbol{\mu}_k)^T \cdot (\mathbf{v}_i - \boldsymbol{\mu}_k)\right) \\
&= \frac{1}{(2\pi)^{D'/2} \sigma_1^{D'}} \exp\left(-\frac{1}{2\sigma_1^2} (\mathbf{v}_i - \boldsymbol{\mu}_k)^T \cdot (\mathbf{v}_i - \boldsymbol{\mu}_k)\right) = \frac{1}{(2\pi)^{D'/2} \sigma_1^{D'}} \exp\left(\frac{(\mathbf{v}_i^\top \cdot \boldsymbol{\mu}_k - 1)}{\sigma_1^2}\right), \quad (16)
\end{aligned}$$

where the last equivalence is because we apply L2 normalization to \mathbf{v}_i and $\boldsymbol{\mu}_k$, respectively. Substituting the corresponding terms in Eq. (14) with Eq. (15) and Eq. (16), and removing the constant terms that are irrelevant to model parameters $\{\theta, \phi, \boldsymbol{\mu}\}$ (note that $p(k) = \frac{1}{K}$), we have:

$$\begin{aligned}
\mathcal{L} &= \frac{1}{|N(i)|} \sum_{j \in N(i)} \frac{1}{2\sigma_2^2} \mathbb{E}_{q_\phi(k | \mathbf{v}_i, \mathbf{z}_j)} [\|\mathbf{v}_i + g_\theta(k) - \mathbf{z}_j\|_2^2] - \mathcal{H}(q_\phi(k | \mathbf{v}_i, \mathbf{z}_j)) \\
&\quad - \frac{1}{|N(i)|} \sum_{j \in N(i)} \mathbb{E}_{q_\phi(k | \mathbf{v}_i, \mathbf{z}_j)} \left[\log \frac{\exp(\mathbf{v}_i^\top \cdot \boldsymbol{\mu}_k / \sigma_1^2)}{\sum_{k'=1}^K \exp(\mathbf{v}_i^\top \cdot \boldsymbol{\mu}_{k'} / \sigma_1^2)} \right] \quad (17) \\
&= \frac{1}{|N(i)|} \sum_{j \in N(i)} \frac{1}{2\sigma_2^2} \mathbb{E}_{q_\phi(k | \mathbf{v}_i, \mathbf{z}_j)} [\|\mathbf{v}_i + g_\theta(k) - \mathbf{z}_j\|_2^2] - \mathbb{E}_{q_\phi(k | \mathbf{v}_i)} \left[\log \frac{\exp(\mathbf{v}_i^\top \cdot \boldsymbol{\mu}_k / \sigma_1^2)}{\sum_{k'=1}^K \exp(\mathbf{v}_i^\top \cdot \boldsymbol{\mu}_{k'} / \sigma_1^2)} \right] - \mathcal{H}(q_\phi(k | \mathbf{v}_i, \mathbf{z}_j))
\end{aligned}$$

$$\begin{aligned}
&= \frac{1}{|N(i)|} \sum_{j \in N(i)} \mathbb{E}_{q_\phi(k|\mathbf{v}_i, \mathbf{z}_j)} [\|\mathbf{v}_i + g_\theta(k) - \mathbf{z}_j\|_2^2] - 2\sigma_2^2 \mathbb{E}_{q_\phi(k|\mathbf{v}_i)} \left[\log \frac{\exp(\mathbf{v}_i^\top \cdot \boldsymbol{\mu}_k / \sigma_1^2)}{\sum_{k'=1}^K \exp(\mathbf{v}_i^\top \cdot \boldsymbol{\mu}_{k'} / \sigma_1^2)} \right] \\
&\quad - \mathcal{H}(q_\phi(k|\mathbf{v}_i, \mathbf{z}_j)),
\end{aligned}$$

where $q_\phi(k|\mathbf{v}_i) = 1/|N(i)| \sum_{j \in N(i)} q_\phi(k|\mathbf{v}_i, \mathbf{z}_j)$. In third line, we multiply the constant $2\sigma_2^2$ for all terms. By absorbing $2\sigma_2^2$ to the hyper-parameter σ_2^2 , we obtain the loss function in Eq. (5).

A.3 Derivation of Global Update

In this section, we derive the analytical global update of prototypes based on our optimization loss over all nodes. Specifically, we have:

$$\begin{aligned}
\boldsymbol{\mu}_k \leftarrow \arg \min_{\boldsymbol{\mu}_k} \sum_{i=1}^N \mathcal{L} &= \arg \max_{\boldsymbol{\mu}_k} \sum_{i=1}^N \mathbb{E}_{q_\phi(k|\mathbf{v}_i)} \left[\log \frac{\exp(\mathbf{v}_i^\top \cdot \boldsymbol{\mu}_k / \sigma_1^2)}{\sum_{k'=1}^K \exp(\mathbf{v}_i^\top \cdot \boldsymbol{\mu}_{k'} / \sigma_1^2)} \right] \\
&= \arg \max_{\boldsymbol{\mu}_k} \sum_{i=1}^N \mathbb{E}_{q_\phi(k|\mathbf{v}_i)} \left[\log \exp(\mathbf{v}_i^\top \cdot \boldsymbol{\mu}_k / \sigma_1^2) \right] \\
&= \arg \max_{\boldsymbol{\mu}_k} \sum_{i=1}^N \mathbb{E}_{q_\phi(k|\mathbf{v}_i)} \left[(\mathbf{v}_i^\top \cdot \boldsymbol{\mu}_k / \sigma_1^2) \right]. \tag{18}
\end{aligned}$$

In the second line, following [48], we treat the normalizing term as the constant. Since we add apply L2 normalization to $\boldsymbol{\mu}_k$: $\|\boldsymbol{\mu}_k\| = 1$, we actually need to solve the Lagrangian of the objective function:

$$\mathcal{L}(\boldsymbol{\mu}_k, \beta) = \max_{\boldsymbol{\mu}_k, \beta} \sum_{i=1}^N \mathbb{E}_{q_\phi(k|\mathbf{v}_i)} \left[(\mathbf{v}_i^\top \cdot \boldsymbol{\mu}_k / \sigma_1^2) \right] + \beta(1 - \boldsymbol{\mu}_k^\top \boldsymbol{\mu}_k). \tag{19}$$

Take the gradient over $\boldsymbol{\mu}_k$ with respect to $\mathcal{L}(\boldsymbol{\mu}_k, \beta)$ and set it to zero, we have:

$$\sum_{i=1}^N q_\phi(k|\mathbf{v}_i) \mathbf{v}_i / \sigma_1^2 - 2\beta \cdot \boldsymbol{\mu}_k = 0 \tag{20}$$

$$\Rightarrow \boldsymbol{\mu}_k = \frac{\sum_{i=1}^N q_\phi(k|\mathbf{v}_i) \cdot \mathbf{v}_i}{2\beta\sigma_1^2} = \frac{\sum_{i=1}^N \pi_i(k) \cdot \mathbf{v}_i}{2\beta\sigma_1^2}, \tag{21}$$

where $\pi_i(k) = q_\phi(k|\mathbf{v}_i) = 1/|N(i)| \sum_{j \in N(i)} q_\phi(k|\mathbf{v}_i, \mathbf{z}_j)$. By taking the gradient with respect to Lagrange multiplier β and setting it to zero, we have: $\boldsymbol{\mu}_k^\top \boldsymbol{\mu}_k = 1$. Combining $\boldsymbol{\mu}_k^\top \boldsymbol{\mu}_k = 1$ and Eq. (21), we have:

$$\beta = \frac{\|\sum_{i=1}^N \pi_i(k) \cdot \mathbf{v}_i\|}{2\sigma_1^2}. \tag{22}$$

Further combining the above equation with Eq. (21), we obtain the analytical global update:

$$\boldsymbol{\mu}_k = \frac{\sum_{i=1}^N \pi_i(k) \cdot \mathbf{v}_i}{\|\sum_{i=1}^N \pi_i(k) \cdot \mathbf{v}_i\|_2}, \text{ where } \pi_i(k) = 1/|N(i)| \sum_{j \in N(i)} q_\phi(k|\mathbf{v}_i, \mathbf{z}_j) \tag{23}$$

Algorithm 1: Training Algorithm of DSSL

Input: $G = (\mathcal{V}, \mathcal{E})$

Output: Online encoder network parameters θ .

Initialize target encoder parameter $\xi = \theta$

repeat

 Randomly select a mini-batch nodes from \mathcal{V}

for each v_i in the batch **do**

 Randomly sample its neighbors $\mathcal{N}(i)$

 Sample c with Gumbel softmax

end

$\mathcal{L} \leftarrow$ Eq. (5)

$[\theta, \phi, \boldsymbol{\mu}] \leftarrow [\theta, \phi, \boldsymbol{\mu}] - \Gamma(\nabla_{\theta, \phi, \boldsymbol{\mu}} \mathcal{L})$

 Update ξ with momentum moving average: $\xi \leftarrow \tau\xi + (1 - \tau)\theta$

until convergence or reaching max iteration;

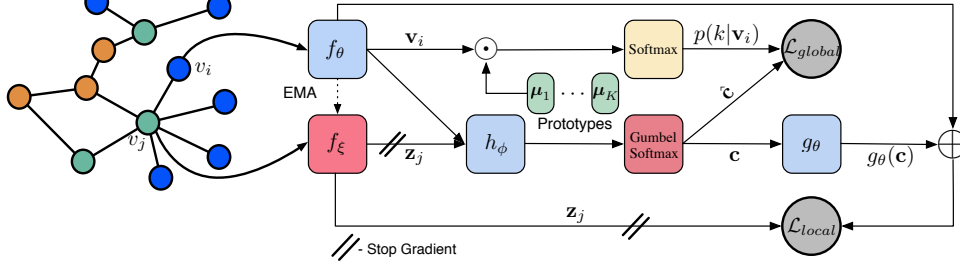


Figure 6: An Illustration of the overall DSSL framework. For simplicity, we only illustrate learning process on one neighbor v_j of central node v_i , while it is applied to all neighbors.

B The Training Algorithm and Network Architecture

B.1 The Training Algorithm of DSSL

The overall training algorithm is shown in Algorithm 1. Concretely, for each iteration of DSSL, we randomly sample the nodes and its neighbors. Then we calculate the loss function with Gumbel softmax approximation. All online trainable parameters are updated with stochastic gradient descent (SGD), while those marked with ξ are the target network counterparts to be updated with exponential moving average.

B.2 The Network Architecture of DSSL

The DSSL framework is illustrated in Figure 6. DSSL proposes a self-supervised scheme that learns to encode the node using an online encoder along with a set of prototypes, inference projector g_θ and predictor h_ϕ . These form the online network. Learning is done by optimizing the local \mathcal{L}_{local} and global \mathcal{L}_{global} losses. To optimize the online parameters, a target encoder is used to produce presentations of neighbors, and updated by exponential moving average. We stop gradients on target encoder coming from the local loss to introduce asymmetry between the online and target encoders.

C Theoretical Analysis

C.1 Proof of Theorem 1

To prove Theorem 1, we first present three Lemmas:

Lemma C.1. *For any random variables X, Y, Z and V , we have the following relations:*

$$I(X, Y; Z|V) \geq I(X; Z|V) \quad (24)$$

Proof.

$$\begin{aligned}
& I(X, Y; Z|V) - I(X; Z|V) \\
&= \iiint \iiint_{XYZV} p(V)p(X, Y, Z|V) \log \frac{p(X, Y, Z|V)}{p(X, Y|V)p(Z|V)} dXdYdZdV \\
&\quad - \iiint \iiint_{XZV} p(X, Z|V) \log \frac{p(X, Z|V)}{p(X|V)p(Z|V)} dXdZdV \\
&= \iiint \iiint_{XYZV} p(X, Y, Z|V) \log \frac{p(X, Y, Z|V)}{p(X, Y|V)p(Z|V)} - p(X, Y, Z|V) \log \frac{p(X, Z|V)}{p(X|V)p(Z|V)} dXdYdZdV \\
&= \iiint \iiint_{XYZV} p(X, Y, Z|V) \log \frac{p(X, Y, Z|V)}{p(Y|X, V)p(X, Z|V)} dXdYdZdV = \\
&\quad \iiint \iiint_{XYZV} p(Y, Z|X, V)p(X|V) \log \frac{p(Y, Z|X)}{p(Y|X, V)p(Z|X, V)} dXdYdZdV = I(Y; Z|X, V) \geq 0. \quad (25)
\end{aligned}$$

This completes the proof of the this Lemma. \square

Lemma C.2. For any random variables Z and X , the mutual information $I(X;Z)$ has a lower bound:

$$\begin{aligned} I(X; Z) &= H(Z) - H(Z|X) = \mathbb{E}_{q(Z)}[\log q(Z)] - \mathbb{E}_{q(Z)q(X|Z)}[\log q(Z|X)] \\ &\geq \max_{\theta} \mathbb{E}_{q(Z)}[\log q(Z)] - \mathbb{E}_{q(Z)q(X|Z)}[\log p_{\theta}(Z|X)], \end{aligned} \quad (26)$$

where $p_{\theta}(Z|X)$ is an introduced variational discriminator with θ representing the parameters.

Proof.

$$\begin{aligned} \mathbb{E}_{q(Z)q(X|Z)}[\log q(Z|X)] &= \max_{\theta} \mathbb{E}_{q(Z)q(X|Z)}[\log p_{\theta}(Z|X)] + KL(q(Z|X)||p_{\theta}(Z|X)) \\ &\geq \max_{\theta} \mathbb{E}_{q(Z)q(X|Z)}[\log p_{\theta}(Z|X)]. \end{aligned} \quad (27)$$

Plugging the inequality above into Eq. (26) completes the proof. \square

Lemma C.3. For any random variables Z and X , the mutual information $I(X, Z)$ has a lower bound:

$$I(X; Z) \geq \mathbb{E}_{p(X,Z)}[f_{\theta}(x, z) - \mathbb{E}_{q(\tilde{\mathcal{B}})}[\log \sum_{z \in \tilde{\mathcal{B}}} \exp f_{\theta}(x, \tilde{z})]] + \log |\tilde{\mathcal{B}}| \quad (28)$$

where x and z are the sample instances, $f_{\theta} \in \mathbb{R}$ is a function parameterized by θ (e.g., a dot product between encoded representations of x and z), and $\tilde{\mathcal{B}}$ is a set of samples drawn from a proposal distribution $q(\tilde{\mathcal{B}})$. The set $\tilde{\mathcal{B}}$ contains the positive sample b and $|\tilde{\mathcal{B}}| - 1$ negative samples.

Proof. The exact derivation of this InfoNCE bound can be founded in [35]. \square

Now, we are ready to prove our Theorem 1. We first restate Theorem 1:

Theorem 1. Optimizing Eq. (5) is equivalent to maximize the mutual information between the node representation \mathbf{v} and the global semantic signal k , and maximize the conditional mutual information between \mathbf{v} and the local signal \mathbf{z} , conditioned on the global signal k . Formally, we have:

$$\max_{\theta, \phi, \mu} \mathcal{L} \Rightarrow \max_{\mathbf{v}} I(\mathbf{v}; k) + I(\mathbf{v}; \mathbf{z}|k) = I(\mathbf{v}; k, \mathbf{z}). \quad (29)$$

Proof. According to Lemma C.1, for any j we have:

$$I(\mathbf{v}, \mathbf{z}|k) = I(\mathbf{v}, \mathbf{z}_1, \dots, \mathbf{z}_{N(v)}|k) \geq I(\mathbf{v}, \mathbf{z}_j|k), \quad (30)$$

which means

$$I(\mathbf{v}, \mathbf{z}|k) = \frac{1}{|\mathcal{N}(v)|} \sum_{j \in \mathcal{N}(v)} I(\mathbf{v}, \mathbf{z}|k) \geq \frac{1}{|\mathcal{N}(v)|} \sum_{j \in \mathcal{N}(v)} I(\mathbf{v}, \mathbf{z}_j|k). \quad (31)$$

For $I(\mathbf{v}, \mathbf{z}_j|k)$, we can relate it to our local loss \mathcal{L}_{local} in the main paper:

$$\begin{aligned} \max_{\mathbf{v}} I(\mathbf{v}, \mathbf{z}_j|k) &\Leftrightarrow \max_{\mathbf{v}} H(\mathbf{z}_j|k) - H(\mathbf{z}_j|k, \mathbf{v}) \\ &\Leftrightarrow \min_{\mathbf{v}, \theta} -\mathbb{E}_{q(\mathbf{v})q(\mathbf{z}_j)q(k|\mathbf{v}, \mathbf{z}_j)}[\log p_{\theta}(\mathbf{z}_j|k, \mathbf{v})] \\ &\Leftrightarrow \min_{\theta, \phi} -\mathbb{E}_{q_{\theta}(\mathbf{v})q_{\xi}(\mathbf{z}_j)q_{\phi}(k|\mathbf{v}, \mathbf{z}_j)}[\log p_{\theta}(\mathbf{z}_j|k, \mathbf{v})] \\ &\Leftrightarrow \min_{\theta, \phi} -\mathbb{E}_{\mathbf{v}=f_{\theta}(\mathbf{g})[v], \mathbf{z}_j=f_{\xi}(\mathbf{g})[j], q_{\phi}(k|\mathbf{v}, \mathbf{z}_j)}[\log p_{\theta}(\mathbf{z}_j|k, \mathbf{v})] \\ &\Leftrightarrow \min_{\theta, \phi} -\mathbb{E}_{\mathbf{v}=f_{\theta}(\mathbf{g})[v], \mathbf{z}_j=f_{\xi}(\mathbf{g})[j], q_{\phi}(k|\mathbf{v}, \mathbf{z}_j)}[\log p_{\theta}(\mathbf{z}_j|k, \mathbf{v})] \\ &\Leftrightarrow \min_{\theta, \phi} \frac{1}{2\sigma_2^2} \mathbb{E}_{q_{\phi}(k|\mathbf{v}, \mathbf{z}_j)}[\|\mathbf{v} + g_{\theta}(k) - \mathbf{z}_j\|_2^2], \end{aligned} \quad (32)$$

where we use Lemma C.1 in the second line and \mathbf{v} and \mathbf{z}_j are the representations of node v and node z_j through deterministic encoder f with input graph $\mathbf{g} = \{\mathbf{X}, \mathbf{A}\}$. Combining Eqs. (32) and (31), we have:

$$\min_{\theta, \phi} \frac{1}{|\mathcal{N}(v)|} \sum_{j \in \mathcal{N}(v)} \frac{1}{2\sigma_2^2} \mathbb{E}_{q_{\phi}(k|\mathbf{v}, \mathbf{z}_j)}[\|\mathbf{v} + g_{\theta}(k) - \mathbf{z}_j\|_2^2] \Rightarrow \max_{\mathbf{v}} I(\mathbf{v}, \mathbf{z}|k). \quad (33)$$

The InfoNCE is related to our global loss. Using Lemma 26 on mutual information $I(\mathbf{v}; k)$, we have:

$$I(\mathbf{v}, k) \geq \mathbb{E}_{p(\mathbf{v}, k)}[f_\theta(\mathbf{v}, k) - \mathbb{E}_{q(\tilde{\mathcal{B}})}[\log \sum_{\tilde{k} \in \tilde{\mathcal{B}}} \exp f_\theta(\mathbf{v}, \tilde{k})] + \log |\tilde{\mathcal{B}}|. \quad (34)$$

When $\tilde{\mathcal{B}}$ always includes all possible values of the latent variable k (i.e., $|\tilde{\mathcal{B}}| = K$) and they are uniformly distributed, and setting $f_\theta(\mathbf{v}, k) = \frac{\mathbf{v}^\top \cdot \boldsymbol{\mu}_k}{\sigma_1^2}$, we have:

$$I(\mathbf{v}, k) \geq \mathbb{E}_{\mathbf{v}=f_\theta(\mathbf{g})[v], q_\phi(k|\mathbf{v}_i)} \left[\log \frac{\exp(\mathbf{v}_i^\top \cdot \boldsymbol{\mu}_k / \sigma_1^2)}{\sum_{k'=1}^K \exp(\mathbf{v}_i^\top \cdot \boldsymbol{\mu}_{k'} / \sigma_1^2)} \right]. \quad (35)$$

Given the above, we have:

$$\max_{\theta, \phi, \boldsymbol{\mu}} \mathbb{E}_{\mathbf{v}=f_\theta(\mathbf{g})[v], q_\phi(k|\mathbf{v}_i)} \left[\log \frac{\exp(\mathbf{v}_i^\top \cdot \boldsymbol{\mu}_k / \sigma_1^2)}{\sum_{k'=1}^K \exp(\mathbf{v}_i^\top \cdot \boldsymbol{\mu}_{k'} / \sigma_1^2)} \right] \Rightarrow \max_{\mathbf{v}} I(\mathbf{v}, k). \quad (36)$$

Combining Eqs. (32) and (36), we have

$$\max_{\theta, \phi, \boldsymbol{\mu}} \mathcal{L} \Rightarrow \max_{\mathbf{v}} I(\mathbf{v}; k) + I(\mathbf{v}; \mathbf{z}|k) = I(\mathbf{v}; k, \mathbf{z}), \quad (37)$$

Omitting the entropy regularization in the loss \mathcal{L} in Eq. (5) completes the proof. \square

C.2 Proof of Theorem 2

To prove Theorem 2, we first present the following Lemmas.

Lemma C.4. *For a representation \mathbf{v} that is obtained with a deterministic GNN encoder f_θ of input graph \mathbf{g} with enough capacity, we have the following data processing Markov chain: $(k, \mathbf{z}) \leftrightarrow \mathbf{y} \leftrightarrow \mathbf{g} \rightarrow \mathbf{v}$.*

Proof. Since \mathbf{v} is a deterministic function of \mathbf{g} , we have the following conditional independence: $(k, \mathbf{z}) \perp \mathbf{v} | \mathbf{g}$ and $\mathbf{y} \perp \mathbf{v} | \mathbf{g}$ [8]. This leads to the data processing Markov chain $(k, \mathbf{z}) \leftrightarrow \mathbf{y} \leftrightarrow \mathbf{g} \rightarrow \mathbf{v}$. \square

Lemma C.5. *By optimizing loss in Eq. (5), the learned representation of \mathbf{v}_{joint} is both minimal and sufficient: \mathbf{v}_{joint} is sufficient $\mathbf{v}_{joint} = \arg \max_{\mathbf{v}} I(\mathbf{v}; k, \mathbf{z})$; \mathbf{v}_{joint} is minimal $\mathbf{v}_{joint} = \arg \min_{\mathbf{v}} H(\mathbf{v}|k, \mathbf{z})$.*

Proof. We further have $I(\mathbf{v}; \mathbf{z}|k) = H(\mathbf{v}|k) - H(\mathbf{v}|k, \mathbf{z})$ in which the entropy $H(\mathbf{v}|k)$ is a constant since $p(\mathbf{v}|k)$ is a Gaussian distribution. Thus, maximizing $I(\mathbf{v}; \mathbf{z}|k)$ is equivalent to minimize $H(\mathbf{v}|k, \mathbf{z})$. Combining this with Theorem 2, we can directly conclude that \mathbf{v}_{joint} is sufficient and minimal. \square

Next, we restate Theorem 2 and provide a complete proof with the help of the Lemmas above.

Theorem 2. *Let $\mathbf{v}_{joint} = \arg \max_{\mathbf{v}} I(\mathbf{v}; \mathbf{z}, k)$, $\mathbf{v}_{local} = \arg \max_{\mathbf{v}} I(\mathbf{v}; k)$, and $\mathbf{v}_{global} = \arg \max_{\mathbf{v}} I(\mathbf{v}; \mathbf{z})$. Formally, we have the following inequalities about the task-relevant information:*

$$I(\mathbf{g}; \mathbf{y}) = \max_{\mathbf{v}} I(\mathbf{v}; \mathbf{y}) \geq I(\mathbf{v}_{joint}; \mathbf{y}) \geq \max(I(\mathbf{v}_{local}; \mathbf{y}), I(\mathbf{v}_{global}; \mathbf{y})) \geq I(\mathbf{g}; \mathbf{y}) - \epsilon. \quad (38)$$

Proof. Based on Lemma C.4, we have the following data processing inequality [42]:

$$I(k, \mathbf{z}; \mathbf{g}) \geq I(k, \mathbf{z}; \mathbf{v}), I(k, \mathbf{z}; \mathbf{g}; \mathbf{y}) \geq I(k, \mathbf{z}; \mathbf{v}; \mathbf{y}), I(\mathbf{g}, \mathbf{y}) \geq I(\mathbf{v}, \mathbf{y}) \quad (39)$$

Since $\mathbf{v}_{joint} = \arg \max_{\mathbf{v}} I(\mathbf{z}, k; \mathbf{v})$, we further have: $I(k, \mathbf{z}; \mathbf{v}_{joint}) = I(k, \mathbf{z}; \mathbf{g})$ and $I(k, \mathbf{z}; \mathbf{v}_{joint}; \mathbf{y}) = I(k, \mathbf{z}; \mathbf{g}; \mathbf{y})$. In addition, since \mathbf{v}_{joint} is minimal, we also have, $I(\mathbf{v}_{joint}; \mathbf{y}|k, \mathbf{z}) \leq H(\mathbf{v}_{joint}|k, \mathbf{z}) = 0$. Give the above, we have the following equality:

$$\begin{aligned} I(\mathbf{v}_{joint}; \mathbf{g}) &= I(\mathbf{v}_{joint}; \mathbf{y}; k, \mathbf{z}) + I(\mathbf{v}_{joint}; \mathbf{y}|k, \mathbf{z}) \\ &= I(\mathbf{g}; \mathbf{y}; k, \mathbf{z}) + I(\mathbf{v}_{joint}; \mathbf{y}|k, \mathbf{z}) \\ &= I(\mathbf{g}; \mathbf{y}; k, \mathbf{z}) + 0 \\ &= I(\mathbf{g}; \mathbf{y}) - I(\mathbf{g}; \mathbf{y}|k, \mathbf{z}) \\ &= \max_{\mathbf{v}} I(\mathbf{v}; \mathbf{y}) - I(\mathbf{g}; \mathbf{y}|k, \mathbf{z}) = I(\mathbf{v}_{sup}; \mathbf{y}) - I(\mathbf{g}; \mathbf{y}|k, \mathbf{z}). \end{aligned} \quad (40)$$

Thus the gap between supervised representation and supervised representation is $I(\mathbf{g}; \mathbf{y}|k, \mathbf{z})$. Based on the property of mutual information, we have:

$$I(\mathbf{g}; \mathbf{y}|k) = I(\mathbf{g}; \mathbf{y}, \mathbf{z}|k) + I(\mathbf{g}; \mathbf{y}|k, \mathbf{z}) \geq I(\mathbf{g}; \mathbf{y}|k, \mathbf{z}). \quad (41)$$

Similarly, we have $I(\mathbf{g}; \mathbf{y}|\mathbf{z}) \geq I(\mathbf{g}; \mathbf{y}|k, \mathbf{z})$. Combining Eqs. (40) and (41), we have the following inequalities about the task-relevant information (note that $I(\mathbf{g}; \mathbf{y}|k, \mathbf{z}) \leq \epsilon$ based on our Assumption 1):

$$I(\mathbf{g}; \mathbf{y}) = \max_{\mathbf{v}} I(\mathbf{v}; \mathbf{y}) \geq I(\mathbf{v}_{\text{joint}}; \mathbf{y}) \geq \max(I(\mathbf{v}_{\text{local}}; \mathbf{y}), I(\mathbf{v}_{\text{global}}; \mathbf{y})) \geq I(\mathbf{g}; \mathbf{y}) - \epsilon, \quad (42)$$

which completes the proof \square

C.3 Proof of Corollary 1

Restate Corollary 1:

Corollary 1. *Suppose that downstream label \mathbf{y} is a M -categorical random variable. Then we have the upper bound for the downstream Bayes errors $P_{\mathbf{v}}^e = \mathbb{E}_{\mathbf{v}} [1 - \max_{y \in \mathcal{Y}} P(\hat{\mathbf{y}} = y|\mathbf{v})]$ on learned representation \mathbf{v} , where $\hat{\mathbf{y}}$ is the estimation for label from our downstream classifier:*

$$\text{Th}(P_{\mathbf{v}_{\text{joint}}}^e) \leq \log 2 + P_{\mathbf{v}_{\text{sup}}}^e \cdot \log M + I(\mathbf{g}; \mathbf{y}|\mathbf{z}, k) \triangleq \text{RHS}_{\mathbf{v}_{\text{joint}}} \quad (43)$$

where $\text{Th}(x) = \min\{\max\{x, 0\}, 1 - 1/|M|\}$ is a thresholded operation [44]. Similarly, we can obtain the error upper bound of other representations $\mathbf{v}_{\text{local}}$ and $\mathbf{v}_{\text{global}}$: $\text{RHS}_{\mathbf{v}_{\text{local}}}$ and $\text{RHS}_{\mathbf{v}_{\text{global}}}$. Then, we have inequalities on error upper bounds: $\text{RHS}_{\mathbf{v}_{\text{joint}}} \leq \min(\text{RHS}_{\mathbf{v}_{\text{local}}}, \text{RHS}_{\mathbf{v}_{\text{global}}})$.

Proof. To prove this Corollary, we use the following inequalities [42, 44]:

$$\text{Th}(P_{\mathbf{v}_{\text{joint}}}^e) \leq -\log(1 - P_{\mathbf{v}_{\text{joint}}}^e) \leq H(\mathbf{y}|\mathbf{v}_{\text{joint}}) \quad (44)$$

$$H(\mathbf{y}|\mathbf{v}_{\text{sup}}) \leq \log 2 + P_{\mathbf{v}_{\text{sup}}}^e \log M. \quad (45)$$

For $H(\mathbf{y}|\mathbf{v}_{\text{joint}})$ and $H(\mathbf{y}|\mathbf{v}_{\text{sup}})$, we have the following relations:

$$\begin{aligned} H(\mathbf{y}|\mathbf{v}_{\text{joint}}) &= H(\mathbf{y}) - I(\mathbf{v}_{\text{joint}}; \mathbf{y}) = H(\mathbf{y}) - I(\mathbf{v}_{\text{sup}}; \mathbf{y}) + I(\mathbf{g}; \mathbf{y}|\mathbf{z}, k) \\ &= H(\mathbf{y}|\mathbf{v}_{\text{sup}}) + I(\mathbf{g}; \mathbf{y}|\mathbf{z}, k), \end{aligned} \quad (46)$$

where we use Eq. (40) in the second equality. Combining Eqs. (44), (45) and (46), we have:

$$\text{Th}(P_{\mathbf{v}_{\text{joint}}}^e) \leq \log 2 + P_{\mathbf{v}_{\text{sup}}}^e \cdot \log M + I(\mathbf{g}; \mathbf{y}|\mathbf{z}, k) \triangleq \text{RHS}_{\mathbf{v}_{\text{joint}}}. \quad (47)$$

Further using that $I(\mathbf{g}; \mathbf{y} | \mathbf{z}, k) \leq I(\mathbf{g}; \mathbf{y}|\mathbf{z})$ and $I(\mathbf{g}; \mathbf{y}|\mathbf{z}, k) \leq I(\mathbf{g}; \mathbf{y}|k)$ in Eq. (41), we have

$$\text{RHS}_{\mathbf{v}_{\text{joint}}} \leq \min(\text{RHS}_{\mathbf{v}_{\text{local}}}, \text{RHS}_{\mathbf{v}_{\text{global}}}), \quad (48)$$

which completes the proof. \square

D Experimental Details

Table 3: Statistics of used graph datasets .

Dataset	# Nodes	# Edges	# Classes	# Features	homophily \hat{h}
Cora	2,708	5,278	7	1,433	.766
Citeseer	3,327	4,552	6	3,703	.627
Pubmed	19,717	44,324	3	500	.664
Texas	183	309	5	1,793	.001
Cornell	183	295	5	1,703	.011
Squirrel	5,201	216,933	5	2,089	.025
Penn94	41,554	1,362,229	2	5	.046
Twitch	9,498	76,569	2	2,545	.142

D.1 Datasets Description and Statistics

In our experiments, we use the following real-world datasets.

Cora, Citeseerm, and Pubmed are citation and high-homophily graphs, which are among the most widely used benchmarks for semi-supervised node classification [25, 13, 45]. In these graphs, nodes are documents, and edges are citations. Each node is assigned a class label based on the research field. The features of each node are represented by a bag of words of its abstracts.

Texas and Cornell are low-homophily graphs representing links between web pages of the corresponding universities and originally collected by the CMU WebKB projects, where nodes and edges represent web pages and hyperlinks, respectively. We use the pre-processed datasets by [32].

Squirrel is the subgraph of web pages in Wikipedia discussing the related topics, collected by [37]. The Squirrel graph is rather complex, with both homophily and heterophily combined.

Penn94 is a friendship network from the Facebook 100 networks of university students from 2005 [27], where nodes represent students and are labeled with the reported gender of students. The node features are major, second major/minor, dorm/house, year, and high school.

Twitch is a graph of relationships between accounts on the streaming platform Twitch. Node features are games liked, location, and streaming habits. Nodes are labeled with the explicit language used by a streamer. We utilize the pre-processed sub-graph Twitch-DE [28]. In Twitch-DE, streamers that do not use explicit content (class 0) also often connect to streamers of class 1, which results in an overall non-homophilous structure.

We utilize the class-average homophily metric proposed recently by [27] to measure the homophily level of graphs. Specifically, the metric is the fraction of edges that connect two nodes of the same class:

$$\hat{h} = \frac{1}{C-1} \sum_{k=0}^{C-1} \left[h_k - \frac{|C_k|}{N} \right]_+, \quad (49)$$

where $[a]_+ = \max(a, 0)$ and C is the total number of classes, and h_k is the class-wise homophily metric:

$$h_k = \frac{\sum_{u \in C_k} d_u^{(k_u)}}{\sum_{u \in C_k} d_u}, \quad (50)$$

in which d_u is the number of neighbors of node u , and $d_u^{(k_u)}$ is the number of neighbors of u that have the same class label. Compared to the edge homophily metric [57], this metric is less sensitive to the number of classes and the size of each class. The statistics of datasets are given in Table 3. We can find that the widely used citation graphs Cora, Citeseer, and Pubmed are highly homophilous, and other graphs show low homophily degrees and thus are non-homophilous.

D.2 Baselines and Implementations

Deepwalk [34] is a network embedding method that generates random walks from all nodes in the graph and then learns latent representations of nodes by treating walks as the equivalent of sentences with SkipGram.

LINE [40] is a network embedding model that preserves both the first-order and second-order proximities.

Struc2vec [36] is embedding method for learning representations for capturing the node structural identity.

GAE [24] is a GCN encoder trained by reconstructing adjacency matrix.

VGAE [24] is a probabilistic version of GAE and is also trained by reconstructing the adjacency matrix.

DGI [46] is an unsupervised node representation method that maximizes the mutual information between node representations and graph summary.

GraphCL [53] is a graph contrastive method that learn node representations by contrasting different augmentations of graphs.

MVGRL [15] is a contrastive learning method by contrasting encoders from neighbors and a graph diffusion.

BGRL [41] is a graph representation learning method that learns node representations by predicting alternative augmentations of the graph.

Table 4: Experimental results (%) on the node classification task with GAT as the encoder. The best and second best performances under each dataset are marked with blue and underline, respectively.

Method	Cora	Citeseer	Pubmed	Texas	Cornell	Squirrel	Penn94	Twitch
MVGRL	84.52 \pm 0.95	71.52 \pm 0.41	81.05 \pm 0.68	53.42 \pm 0.29	50.29 \pm 0.96	37.58 \pm 0.95	57.21 \pm 0.30	67.11 \pm 0.23
BGRL	83.91 \pm 0.25	<u>72.15</u> \pm 0.42	80.12 \pm 0.52	51.02 \pm 1.10	48.97 \pm 1.03	35.33 \pm 1.12	56.52 \pm 0.25	66.21 \pm 0.33
DSSL	82.54 \pm 0.46	73.67 \pm 0.68	81.69 \pm 0.37	59.73 \pm 1.28	53.63 \pm 1.16	39.42 \pm 1.34	58.97 \pm 0.26	69.55 \pm 0.48

Table 5: Experimental results (%) with standard deviations on the node clustering task. The best and second best performance under each dataset are marked with blue and underline, respectively.

Method	Cora	Citeseer	Pubmed	Texas	Cornell	Squirrel	Penn94	Twitch
Deepwalk	31.15 \pm 0.05	31.23 \pm 0.06	34.59 \pm 0.09	16.90 \pm 0.13	10.23 \pm 0.18	16.97 \pm 0.13	13.24 \pm 0.16	25.08 \pm 0.14
LINE	33.78 \pm 0.03	33.37 \pm 0.04	38.31 \pm 0.06	18.61 \pm 0.15	13.57 \pm 0.14	<u>18.59</u> \pm 0.12	14.49 \pm 0.09	26.81 \pm 0.07
Struc2vec	20.17 \pm 0.05	19.31 \pm 0.08	15.13 \pm 0.03	22.14 \pm 0.10	9.18 \pm 0.12	<u>14.85</u> \pm 0.15	12.58 \pm 0.17	22.49 \pm 0.14
GAE	37.43 \pm 0.05	32.45 \pm 0.05	34.38 \pm 0.06	26.97 \pm 0.11	15.39 \pm 0.13	11.73 \pm 0.08	16.70 \pm 0.15	27.45 \pm 0.17
VGAE	38.92 \pm 0.08	36.49 \pm 0.03	41.09 \pm 0.04	27.75 \pm 0.16	17.87 \pm 0.13	10.83 \pm 0.09	17.34 \pm 0.08	25.89 \pm 0.08
DGI	45.17 \pm 0.08	42.03 \pm 0.08	45.33 \pm 0.02	<u>34.17</u> \pm 0.07	15.92 \pm 0.15	8.49 \pm 0.13	12.14 \pm 0.19	25.84 \pm 0.18
GraphCL	46.29 \pm 0.03	46.38 \pm 0.12	46.78 \pm 0.03	30.25 \pm 0.13	16.86 \pm 0.17	7.97 \pm 0.13	16.35 \pm 0.13	27.55 \pm 0.16
MVGRL	48.65 \pm 0.07	45.33 \pm 0.02	<u>48.81</u> \pm 0.21	32.72 \pm 0.18	18.02 \pm 0.11	17.65 \pm 0.08	15.80 \pm 0.17	24.53 \pm 0.16
BGRL	<u>47.35</u> \pm 0.03	44.78 \pm 0.04	47.21 \pm 0.07	33.59 \pm 0.15	<u>19.74</u> \pm 0.14	15.13 \pm 0.09	<u>17.49</u> \pm 0.13	25.69 \pm 0.09
DSSL	46.77 \pm 0.04	47.89 \pm 0.04	49.39 \pm 0.02	38.22 \pm 0.15	20.36 \pm 0.08	19.85 \pm 0.13	18.66 \pm 0.15	29.63 \pm 0.08

We used the official implementation publicly released by the authors on Github for all baselines. We ran our experiments on GeForce RTX 2080 Ti. In all our experiments, we use the Adam optimizer [22]. The projector g_θ and predictor h_ϕ are both the Multilayer Perceptron (MLP) with a single hidden layer. We also used stabilization techniques like batch normalization on Penn94 and Twitch datasets for all methods. We use ReLU activation in all experiments.

D.3 Experimental setup

We use the same dataset splits and training procedure for all methods. We tune hyper-parameters for all models individually and randomly initialize the model parameters. For all methods, the hyper-parameter search spaces are as follows: learning rate $\{0.001, 0.005, 0.01\}$, representation dimension $\{16, 32, 64\}$, L2 weight-decay $\{5e-4, 1e-4, 5e-6, 1e-6\}$. For our DSSL, we tune the following hyper-parameters: $\sigma_1^2 \in \{0.2, 0.4, 0.6, 0.8, 1.0\}$, $\sigma_2^2 \in \{0.2, 0.4, 0.6, 0.8, 1.0\}$, $\lambda \in \{0.2, 0.4, 0.6, 0.8, 1.0\}$ and $K \in \{2, 4, 6, 8, 16, 32\}$.

E Additional Experimental Results

E.1 Results with Other Encoders

To further evaluate the effectiveness of the proposed DSSL, we consider the case where the learning method is implemented using another GNN encoder. Table 4 shows the results of the selected baseline with GAT as the encoder. As shown in Table 4, our DSSL performs better than all the compared methods in most cases, which once again proves the effectiveness of DSSL and also shows that DSSL is robust to various encoders.

E.2 Node Clustering Results

We provide the node clustering results in Table 5. As shown in Table 5, we can find that our DSSL can consistently improve the node clustering performance compared to the baselines on all datasets except the Cora. This observation once again verifies the effectiveness of DSSL in learning generalizable node representations. In addition, along with the node classification performance, these results show that DSSL can provide transferable and robust node representations for various downstream tasks.

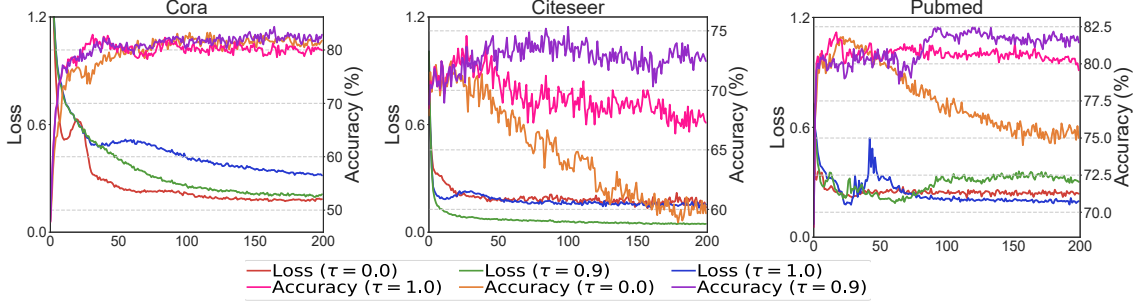


Figure 7: Performance on Cora, Citeseer and Pubmed with varying τ .

E.3 Additional Results on Ablation Study and Parameter Analysis

Ablation Study. We further conduct experiments to study the effects of the global update on prototypes and asymmetric architecture on homophily datasets. Figures 7 and 9 show the ablation results on Cora, Citeseer and Pubmed. These results also echo the collapse issue as discussed in the main text: without the global update and asymmetric architecture, there is significant performance drop on these three homophily datasets.

Parameter Analysis. We provide more results on the parameter analysis. Figure 8 shows the results on Citeseer, Cornell, and Squirrel datasets. We can observe that having large values of σ_2^2 also does not improve the overall performance, and DSSL is not very sensitive to the Gumbel softmax temperature λ for these three datasets. We also find that as K increases from 2 to 8 (2 to 16 for Citeseer), the accuracy of DSSL improves.

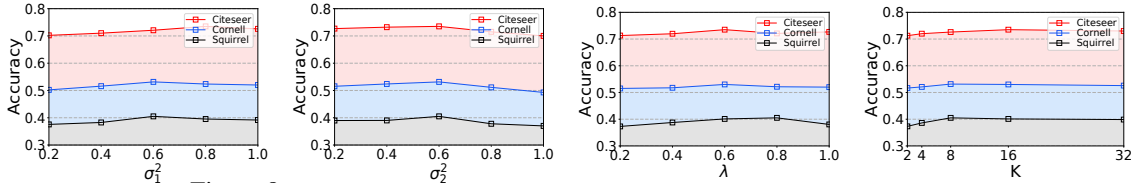


Figure 8: Hyper-parameter analysis on Citeseer, Cornell and Squirrel datasets.

E.4 Additional Results on Visualization and Case Study

To further examine the learned latent factors, in Figure 10, we provide the additional case study results on other datasets. We can find that, in most cases, the latent factors share a similar distribution for the same type of link, which illustrates its effectiveness in decoupling the underlying latent semantic meaning of different neighbors. This also interprets the reason why capturing the semantic shift can improve performance.

F Discussion and Broader impact

In this paper, we proposed a new framework called decoupled self-supervised learning (DSSL) for unsupervised node representation learning on non-homophilous graphs. Compared with other contrastive learning methods, our DSSL does not need prefabricated augmentations. The theoretic analysis and extensive experiments show the effectiveness of our proposed DSSL.

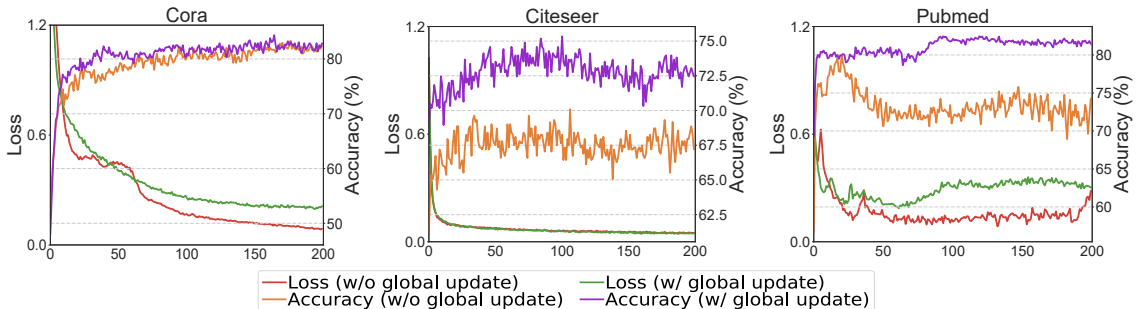


Figure 9: Performance on Cora, Citeseer and Pubmed w and w/o global update.

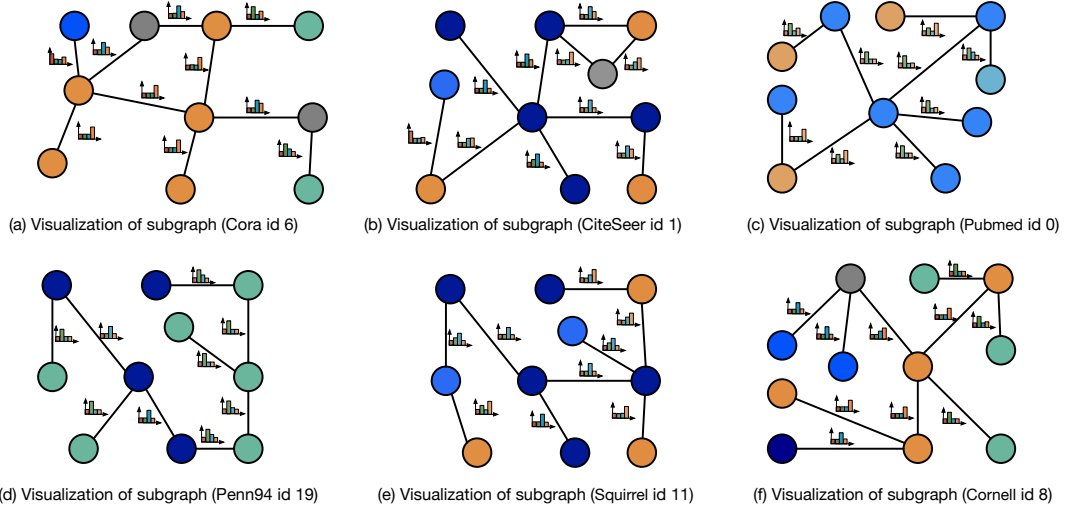


Figure 10: The visualization and case study results on other datasets. (best viewed on a computer screen and note that the latent distribution of each link need to be zoomed in to be better visible).

Limitation of the work. Despite the theoretical grounds and the promising experimental justifications, there is one limitation of the current work which we hope to improve in future work: our theoretic analysis requires some assumptions on the relationship between the downstream labels and the neighborhood distribution (Assumption 1). While, not surprisingly, we have to make some assumptions to expect good generalization for the unsupervised node representation learning, it is an interesting future direction to explore more relaxed assumptions than the ones used in this work.

Potential negative societal impacts. In this work, we propose a self-supervised learning framework for node representation learning which does not rely on annotated labels, which might reduce the need for label annotation and thus makes a few individuals who focus on labeling or annotating data unemployed. In addition, our learned representation may suffer from malicious adversaries who seek to extract node-level information about sensitive attributes. Thus, the robustness of DSSL could be further improved to prevent attacks from an adversary.